# Optimization of a Servo Motor for an Industrial Robot Application

Svante Andersson

Lund 2000

Department of
Industrial Electrical Engineering and Automation
Lund Institute of Technology
Lund University
P.O. Box 118
S-221 00 LUND
SWEDEN

**http://www.iea.lth.se**

ISBN 91-88934-15-2
CODEN:LUTEDX/(TEIE-1023)/1-112/(2000)


Printed in Sweden by Universitetstryckeriet, Lund University

# Abstract

A permanent magnet synchronous machine has been optimized for an industrial robot application. The optimization was made with respect to material cost, considering the demands of the application. In the optimization, drive cycle information was utilised, and the effect of the inertia of the machine was considered. A simple magnetic equivalent circuit was used to calculate the no load flux, and the finite element method was used for the calculation of torque ripple and induced voltage. Root mean square values for the speed and the torque profiles of the drive cycle was used for the calculation of the iron and copper losses. The optimization yielded a smaller and less expensive machine, compared to the machine presently used in the application. The active length was reduced by 35 %, the inertia of the active part of the machine was reduced by 56 %, and the material cost of the active part of the machine was reduced by 30 %. The new machine has a novel design of the rotor and a simple magnet geometry. FEM calculations indicate that the machine has a high torque ripple, and it is assumed that this can be compensated for by current profiling. A prototype has been built and measurements show a very good agreement with finite element calculation results. The prototype has, due to an error in the manufacturing of the magnets, slightly inferior thermal properties to fulfil the demands of the drive cycle.

# Acknowledgements

This work has been carried out at the department of Electrical Industrial Engineering and Automation, Lund Institute of Technology, Lund, Sweden. It has been a part of a project sponsored by API-ELMO AB, ABB Robotics AB and the Swedish National Board for Industrial and Technical Development (NUTEK). Their support is hereby gratefully acknowledged.

A number of people earn my gratitude for their support during my work.

First of all I would like to thank Professor Mats Alaküla for supervision and the opportunity to work on this project. I am also very thankful for his patience with delays and postponed dead-lines.

I would like to thank Mr Erik Ramsel and Mr Tommy Lejonberg at API-ELMO AB in Flen, Sweden, for all help, information and ideas. The concept of the tube-rotor employed by the prototype originates from Mr Lejonberg.

I also wish to thank Mr Jesper Bergsjö and Mr Ove Kullborg at ABB Robotics AB in Västerås, Sweden, for valuable information regarding the dimensioning of servo motors for industrial robots. Their the technical expertise has been of great value in the project.

I would like to express my sincere gratitude to Dr Robert Bjärnemo and Dr Åke Burman at the Department of Machine Design, LTH, for their unselfish and generous assistance to a PhD-student from another department. I am most grateful to Dr Bjärnemo for letting me use both hardware and software for the FEM calculations. Without the assistance of Dr Bjärnemo, this work had been both more difficult and of less quality, as our department has been lacking a suitable FEM-program during almost the whole of my project. Dr Burman gave invaluable advice on using the FEM software, and without Dr Burmans help the FEM-calculations would not have been near the speed and usefulness that they have reached today. I am also very grateful for his his patience with filled disks and forgotten passwords.

Thanks also to Dr Anders Eriksson at ABB Corporate Research AB in Västerås, Sweden, for answering my numerous questions regarding the FEM-software.

I am very thankful to Mr Martin Satur and Mr Allan Alcott at Swift-Levick Magnets Ltd in Barlborough, England, for the advice regarding the gluing of magnets and the explanation of the phenomena of the varying magnet strength.

I am most grateful to Mr Morten Hemmingsson for his generous and rapid help with LaTeX.

I would also like to thank Mr Peter Thelin and Mr Joachim Lindström for interesting discussions regarding permanent magnet motor design and testing.

Thanks also to Dr Tord Cedell for his helpful assistance with measuring the BH-curves for the rotor material.

I would also like to thank Mr Per Karlsson, Mr Håkan Skarrie, Mr Morten Hemmingsson and Ms Karin Jonasson for their valuable comments on the thesis.

Finally I would like to thank my family for all the support they have given me during this project.

Lund, May 2000

*Svante Andersson*

# Contents


**1. Introduction** . . . . . 1
- 1.1 Background . . . . . 1
- 1.2 Outline of the thesis . . . . . 3

**2. The application and the machine** . . . . . 5
- 2.1 Demands on a servo motor in an industrial robot application 5
- 2.2 Axis 5 in IRB4400 . . . . . 5
- 2.3 Drive cycle . . . . . 5
- 2.4 General design of a PMSM . . . . . 9
- 2.5 Control . . . . . 11
- 2.6 Separation of losses . . . . . 14
- 2.7 Torque quality . . . . . 15
- 2.8 Magnets . . . . . 16
- 2.9 The present design . . . . . 17

**3. The design model** . . . . . 19
- 3.1 Concepts of a new machine . . . . . 19
- 3.2 Program environment . . . . . 21
- 3.3 The sequence of the calculations . . . . . 21
- 3.4 Parametrization of the geometry . . . . . 22
- 3.5 Calculation of flux . . . . . 23
- 3.6 Calculation of inertia . . . . . 29
- 3.7 Calculation of necessary torque . . . . . 30

3.8 Calculation of necessary current . . . . . 31
3.9 Calculation of copper losses . . . . . 32
3.10 Calculation of iron losses . . . . . 33
3.11 Thermal considerations . . . . . 33
3.12 Magnet protection . . . . . 34
3.13 Calculation of the constraints . . . . . 34
3.14 Calculation of the material cost . . . . . 36
3.15 Comments on the design model . . . . . 37

**4. Optimization** . . . . . 41
4.1 Optimization strategy . . . . . 41
4.2 Parameters for the optimization . . . . . 44
4.3 Comparison of pole numbers . . . . . 46
4.4 Torque ripple calculations by FEM . . . . . 47
4.5 Optimization of ten-pole design . . . . . 48
4.6 Comparison of the designs . . . . . 50
4.7 Magnet shape . . . . . 50
4.8 FEM calculations on final design . . . . . 51

**5. The Prototype** . . . . . 59
5.1 The stator . . . . . 59
5.2 The rotor . . . . . 60
5.3 Magnets . . . . . 61
5.4 Recalculation of drive cycle requirement . . . . . 68
5.5 Data for the optimized geometry . . . . . 70
5.6 Comparison old and new design . . . . . 70

**6. Measurements** . . . . . 75
6.1 Standard Thermal Test . . . . . 75
6.2 The laboratory setup . . . . . 76
6.3 The induced voltage . . . . . 78
6.4 Torque . . . . . 79
6.5 Inductance measurements . . . . . 80

6.6 Thermal limit measurements . . . . . 81
6.7 Comments . . . . . 82

**7. Conclusions and Future Work** . . . . . 83
7.1 Conclusions . . . . . 83
7.2 Future work . . . . . 85

**8. References** . . . . . 87

**A. Magnet data** . . . . . 89

**B. Calculation of iron losses** . . . . . 91

**C. Demagnetization margin** . . . . . 95
C.1 Magnet property . . . . . 95
C.2 Maximum demagnetizing current . . . . . 96
C.3 Minimum magnet height . . . . . 97

**D. Thermal constraints** . . . . . 99

**E. Test flange** . . . . . 101

# 1

# Introduction

## 1.1 Background

Industrial robots are today in widespread use in the industry, performing tasks such as welding, machine tending, material handling, grinding, packaging and assemblage. The car industry and its sub-contractors, but also to an increasing extent, the food industry, are extensive users of industrial robot technology. In 1974, the worlds first all-electric industrial robot was delivered by Asea. The first robots were equipped with *Direct Current* machines (DC-machines), which had limited overload capacity, and need for maintenance. In 1986, Asea introduced robots utilizing permanent magnet synchronous motors (PMSM). The benefit of the PMSM, compared to the DC-machine, is its lower price and minimum need of maintenance. PMSM is today the dominating technology. The control of the PMSM, however, is more complex. At the time of the introduction of PMSM's in industrial robots, the electronics were putting constraints on the maximum sample time, which lead to quite low maximum electric frequencies. This was necessary to avoid torque ripple induced by the converter, so the pole numbers were kept to four and six, even if it had been beneficial with higher pole numbers, from a machine design point of view. Today, the electronics can cope with much higher frequencies, so the constraint of the electronics on the pole number is no longer present.

The general trend on the industrial robot market today is a frequent introduction of new models and a high sensitivity to price. This leads to a continuous demand for cost reduction and rapid development of new products. This demand of course also applies to the sub-suppliers, the manufacturers of servo motors.

The electric drive system is an important part of the robot, and servo motors

are key components. Therefore competence in the field of electric machine design is essential to the manufacturers of industrial robots and their suppliers of servo motors.

A drive cycle can characterize the demands on a servo motor in an industrial robot. The drive cycle usually consist of an acceleration, a part with constant speed, a retardation and standstill.

As machines of this kind in this application are thermally limited, i.e. what will destroy a machine is overheating, the rating of the machine has to be done with respect to the thermal capacity, not necessarily the nominal torque.

The drive cycle usually has a low intermittence, i.e. the motor has to supply high torque during the cycle, but only during a small fraction of the total cycle time. The losses are large when the motor is producing high torque, but as they are produced under a fraction of the cycle time, the average losses will be lower. The thermal time constant of the motor is much longer than the cycle time of a drive cycle, and therefore the average losses during a cycle can be used for determining the necessary rating of the motor. The peak torque during the drive cycle can therefore be substantially higher than the rated torque of the motor. By sizing the motor considering the thermal demands instead of the peak torque during the cycle, a smaller and less expensive machine can accomplish the desired task.

The inertia of the motor is very important in all servo drives, as during the acceleration, the motor not only has to supply torque to accelerate the load, but also has to supply the torque to accelerate itself. What is important is the ratio between the motor inertia and the load inertia. If the motor inertia is negligible compared to the load inertia, the benefit of reducing the motor inertia is small, as most of the motor torque anyway is used to accelerate the load. On the other hand, if the motor and load inertia are of comparable sizes, reducing the motor inertia will give the benefit of less torque requirement for the same acceleration.

It is important that a servo motor produces little or negligible torque ripple. Torque ripple is practically always reduced in the machine design, but unfortunately these measures reduces the rated torque of the machine, and a trade off has to be made between average torque and torque ripple. There is, however, also the possibility of shaping the currents so that even a machine that produces significant torque ripple when connected to a conventional supply, produces no, or little, torque ripple when fed with the proper currents. Then a smaller and less expensive machine can produce the same average torque with the same torque ripple. There will be higher demands on the electronics, however, so a trade off has to be made between the amount of motor material and the complexity of the electronics.

The servo motor to be optimized is the PS90/6-131, manufactured by APH-ELMO AB in Flen, Sweden. It is among other applications used in the industrial robot IRB4400 manufactured by ABB Robotics AB in Västerås, Sweden. The optimization is done for axis 5 in the robot, which is the hand joint.

When optimizing an electric machine, there are different criteria of the optimum to choose from, for example minimum weight, minimum cost, maximum torque etc. To every criteria of optimum there must be constraints like minimum permissible torque, maximum allowable volume etc. Here, the criteria of the optimum has been chosen to be to *minimize the material cost of a machine capable of performing a specific task*. The material cost is the *object function* and the demands of the drive cycle, together with some geometric conditions, are the constraints. The inertia of the motor is included in the optimization.

## 1.2 Outline of the thesis

In chapter 2, the demands of a servo motor in an industrial robot application is described, and a typical drive cycle is presented. The chapter also includes design features of the *permanent magnet synchronous machine* (PMSM), the control of PMSM's, a brief overview of the different magnet materials utilized in PMSM's today, and a presentation of the present design. The concept of separation of iron and copper losses is introduced.

In chapter 3 the model of the machine, used in the optimization, is presented.

In chapter 4 the optimization is described with respect to strategy, order of calculations and results. The *finite element method* (FEM) results are also presented.

In chapter 5 the manufacturing of the prototype is described, and the tests and measurements on the prototype are presented in chapter 6.

Finally, chapter 7 presents some conclusions.

# 2

# The application and the machine

## 2.1 Demands on a servo motor in an industrial robot application

The demands on a servo motor in an industrial robot application is to have high torque quality and low price. Ability to deliver high peak torque, 2-4 times the nominal torque, with maintained torque quality is also important. Little or no need for maintenance is a requirement.

Torque quality means smooth and exact torque regardless of temperature and operating point. Low price means high torque per unit price, $Nm/\$$.

## 2.2 Axis 5 in IRB4400

The object of the optimization is the motor for axis 5 in ABB's industrial robot IRB4400, see figure 2.1. The robot is a medium size industrial robot, mainly used for material handling, and a payload of up to 60 kg. The robot has 6 axes in total, and axis 5 is the tilt axis for the hand joint, see figure 2.1. The motor for axis 5 is, however, mounted in the rear of the the robot arm, see figure 2.1. The torque and rotational movement is translated from the motor to the axis via shafts and gears in the robot arm.

## 2.3 Drive cycle

A typical cycle for a servo motor in an industrial robot is shown in figure 2.2.

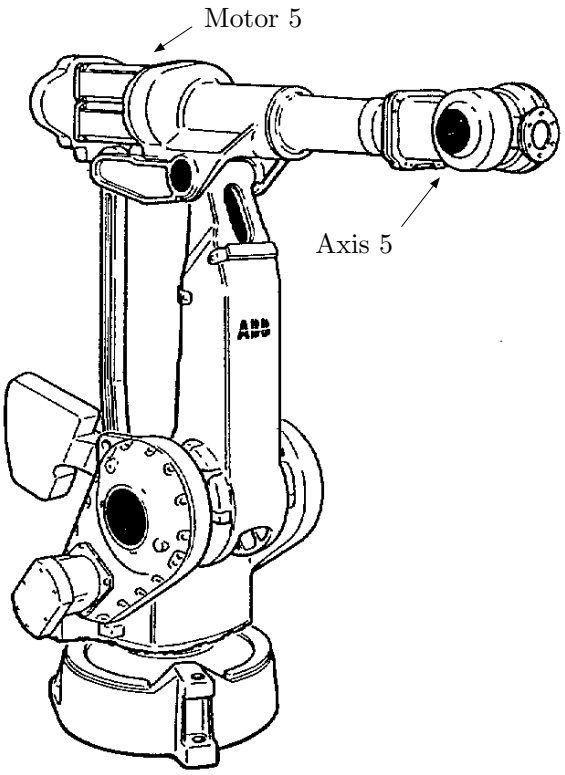


**Figure 2.1** The IRB4400

If the robot is going to move a piece from one place to another, the axes should as fast as possible reach their maximum speed, keep that speed until near the destination, and then brake down to standstill. A short standstill period is needed for releasing the piece and/or gripping a new piece. Initially in the cycle, the motor has to supply a high accelerating torque, $T_{acc}$, to accelerate the axis up to maximum speed. When maximum speed is reached, a lower, constant torque, $T_{stat}$, is applied during the constant speed period, and then a high braking torque, $T_{dec}$, during the braking to standstill. During the standstill a constant torque, $T_{stat}$, is again supplied. A representative drive cycle for each of the axes can however be constructed, and it will consist of an acceleration, a period of constant speed and braking to zero speed. The time for the whole of such cycle is just a few seconds which is much shorter than the thermal time constant of the machine. A mechanical equivalent diagram

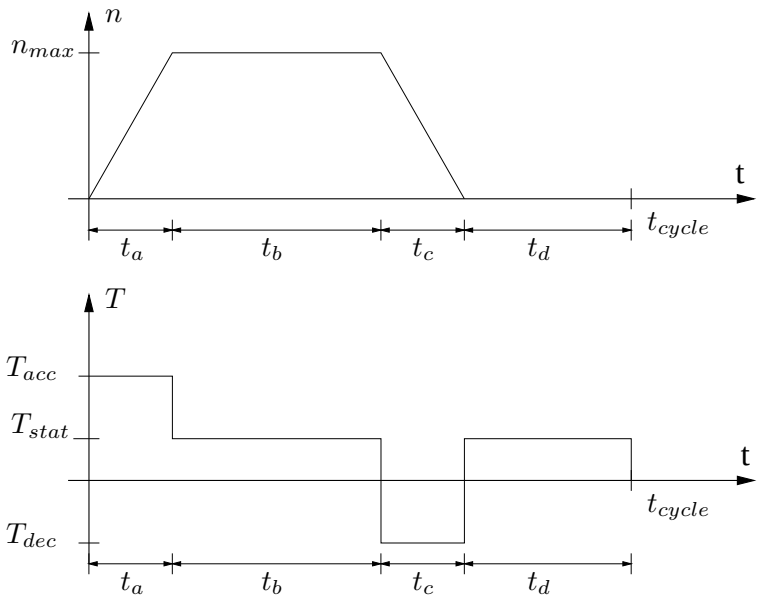


**Figure 2.2** A typical cycle for a servo motor in an industrial robot.

of the servo motor, the gear and the load is shown in figure 2.3. The load inertia, $J_{load}$, includes both the payload and the robots own structure. The load inertia referred to the motor side of the gear is designated the equivalent load inertia, $J_{load-eq}$, and equals the load inertia multiplied with the square of the gear ratio. The gear is designed for a maximum allowed torque, $T_{gear}$, on the motor side which must not be exceeded, for mechanical reasons. The maximum acceleration $\left(\frac{d\omega}{dt}\right)_{max}$ is then determined as

$$\left(\frac{d\omega}{dt}\right)_{max} = \frac{T_{gear}}{J_{load-eq}} \tag{2.1}$$

If the inertia of the motor is negligible, the maximum allowed gear torque puts an upper limit to the torque the motor has to supply. If the inertia of the motor is not negligible, however, the motor must supply not only the maximum gear torque, but also the necessary torque to accelerate itself with $\left(\frac{d\omega}{dt}\right)_{max}$. A motor with lower inertia thus has to produce less torque for the same acceleration. In this way, the acceleration torque and braking torque

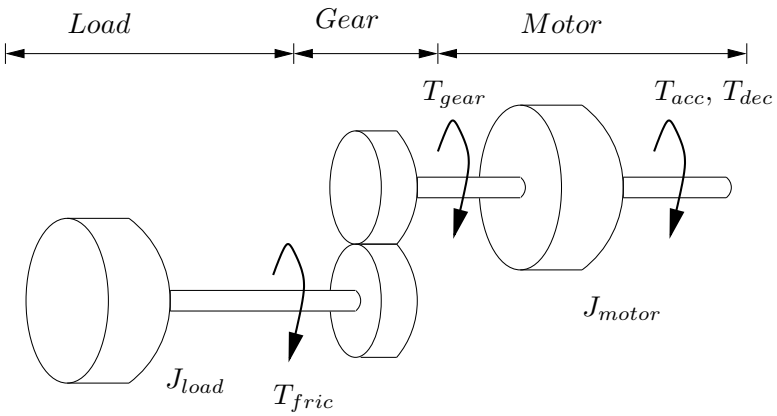


**Figure 2.3** A mechanical equivalent of the servo motor, the gear and the load.

can then be calculated.

$$T_{acc} = T_{gear} + T_{fric} + J_{motor}\left(\frac{d\omega}{dt}\right)_{max} \tag{2.2}$$

$$T_{dec} = T_{gear} - T_{fric} + J_{motor}\left(\frac{d\omega}{dt}\right)_{max} \tag{2.3}$$

$T_{fric}$ is the friction torque on the motor side of the shaft, the friction in the gear on the motor side, and the friction in the motor itself. As the sign $T_{fric}$ is depending on the sign of the speed, $T_{fric}$ remains positive during one cycle according to figure 2.2. $T_{acc}$ thus becomes larger than $T_{dec}$ as the motor is aided by the friction during braking. For the drive cycle of figure 2.2 the static torque, $T_{stat}$, the maximum allowed gear torque, $T_{gear}$, the friction torque, $T_{fric}$, and the equivalent load inertia, $J_{load-eq}$, are specified. If the motor inertia is known, the required torque during a drive cycle can be calculated with equations 2.2 and 2.3. The intermittence, $i$, is the fraction of time the motor is accelerating or braking during a drive cycle. It is calculated, using the notation in figure 2.2, as

$$i = \frac{t_a + t_c}{t_{cycle}} \tag{2.4}$$

A low intermittence means that the time during which the motor is accelerating or braking is short compared to the cycle time. This means that without overheating the motor, the peak torque during the drive cycle can be substantially higher than the rated torque of the motor. In an industrial

robot application, the intermittence is quite low, about 10%, so selecting a machine with rated torque equal the peak torque will yield a much larger machine than necessary. A permanent magnet synchronous machine with surface mounted magnets can often cope with large torque peaks while maintaining the torque constant, i.e. the linear relationship between current and torque is maintained even during torque peaks several times the nominal torque. A root mean square torque, $T_{rms}$, a root mean square speed, $n_{rms}$, and an average speed, $\overline{n}$, can be calculated with the above information.

$$T_{rms} = \sqrt{\frac{1}{t_{cycle}} \int_0^{t_{cycle}} T^2(t)\ dt} \tag{2.5}$$

$$n_{rms} = \sqrt{\frac{1}{t_{cycle}} \int_0^{t_{cycle}} n^2(t)\ dt} \tag{2.6}$$

$$\overline{n} = \frac{1}{t_{cycle}} \int_0^{t_{cycle}} n(t)\ dt \tag{2.7}$$

## 2.4 General design of a PMSM

In a *permanent magnet synchronous machine*, *PMSM*, the stator phase voltages and currents are ideally sinusoidal. The flux in the machine is mainly set up by the permanent magnets in the rotor, which ideally produce a sinusoidally distributed flux in the airgap

There are different ways of mounting the magnets on the rotor, in figure 2.4 machines with surface mounted magnets, inset magnets and buried magnets are shown. Depending on the configuration, different properties of the machine are obtained. With surface mounted magnets, see figure 2.4(a), the rotor iron is approximately round and the stator inductance is low, as well as independent of the rotor position. The control of the machine becomes simple, as no account has to be taken for the reluctance effects. Field weakening is difficult due to the low stator inductance, and thus operation above base speed becomes difficult.

With inset magnets, see figure 2.4(b), the stator inductance becomes position dependent. During field weakening, a certain amount of reluctance torque is obtained, making operation above base speed more feasible. This configuration is popular in PMSM:s intended for traction applications, where operation above base speed is frequent.

With buried magnets, see figure 2.4(c), flux concentration is possible, i.e. that the flux density in the airgap can be higher than in the magnets. Low

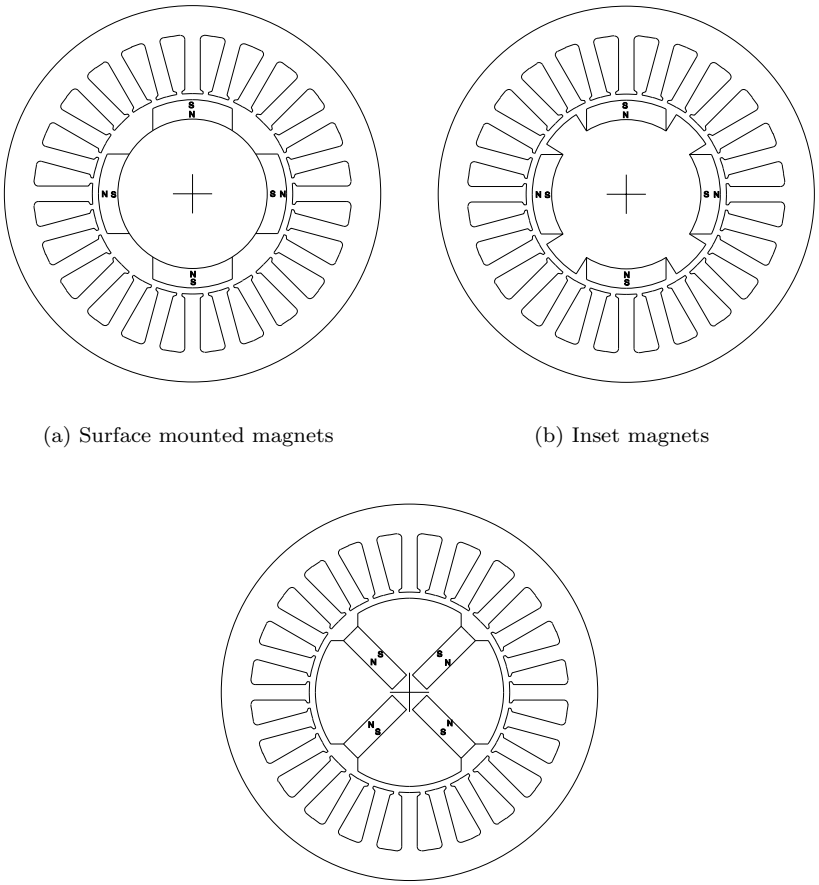

(a) Surface mounted magnets

(b) Inset magnets

(c) Buried magnets

**Figure 2.4** Different ways of mounting the magnets on the rotor. Depending on the configuration, different properties of the machine are obtained.

energy magnets (Ferrites, see below) can thus be used and still obtain a high torque density.

A very good reference regarding the practical issues of PMSM design is [10].

## 2.5 Control

Control of the machine can be made with different algorithms, in either a stationary or a synchronous reference frame, see [12] and [11]. A popular method is vector control in synchronous coordinates, which today is used in industrial robots for the control of the servo motors considered here.

To be able to have constant reference values for the currents, control is performed in a reference frame rotating synchronously with the rotor, see figure 2.5.

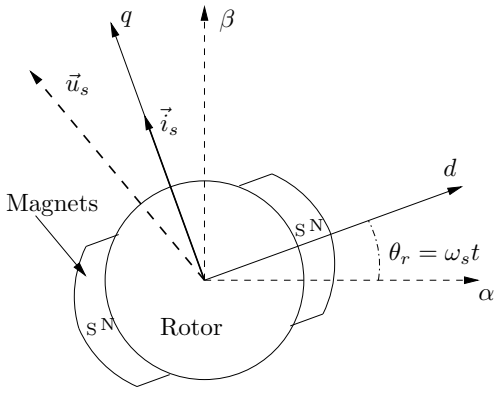


**Figure 2.5** The rotor oriented coordinate system, $dq$, rotating synchronously with the rotor, and the stationary coordinate system, $\alpha\beta$. With *quadrature current control*, the current vector is always aligned with the $q$-axis.

Only the fundamental of the flux and current distribution in the machine is considered. The electrical equation for the stator winding of a PMSM can then be written in vector form

$$\vec{u}_s^{\,\alpha\beta}(t) \quad = \quad R_s \vec{i}_s^{\,\alpha\beta}(t) + \frac{d\vec{\psi}_s^{\,\alpha\beta}(t)}{dt} \tag{2.8}$$

The superscript $\alpha\beta$ denotes stationary coordinates. This equation can then be transformed into a synchronous reference frame, $dq$-coordinates, with the

real axis aligned with the peak of the fundamental component of the magnet flux. The synchronous reference frame is rotating with the electrical speed of the rotor, $\omega_s$, so the stator voltage equation in synchronous coordinates will be

$$\vec{u}_s^{\,dq}(t) = R_s \vec{i}_s^{\,dq}(t) + \frac{d\vec{\psi}_s^{\,dq}(t)}{dt} + j\omega_s \vec{\psi}_s^{\,dq}(t) \tag{2.9}$$

An additional term due to the rotation, $j\omega_s \vec{\psi}_s^{\,dq}(t)$, is added to the equation. The real, $d$, and imaginary, $q$, parts can be separated.

$$u_{sd}(t) = R_s i_{sd}(t) + \frac{d\psi_{sd}(t)}{dt} - \omega_s \psi_{sq}(t) \tag{2.10}$$

$$u_{sq}(t) = R_s i_{sq}(t) + \frac{d\psi_{sq}(t)}{dt} + \omega_s \psi_{sd}(t) \tag{2.11}$$

The expressions for the flux linkage in the $d$ and $q$-directions are

$$\psi_{sd} = \psi_m + L_{sd} i_{sd} \tag{2.12}$$

$$\psi_{sq} = L_{sq} i_{sq} \tag{2.13}$$

$L_{sd}$ and $L_{sq}$ are the stator inductances in the $d$ and $q$-directions respectively. Combining equations 2.10 to 2.13, in combination with the assumption that the fundamental component of the magnet flux stays constant, i.e. $\frac{d}{dt}(\psi_m) = 0$, yields

$$u_{sd}(t) = R_s i_{sd}(t) + \frac{d}{dt}\Big(L_s i_{sd}(t)\Big) - \omega_s L_s i_{sq}(t) \tag{2.14}$$

$$u_{sq}(t) = R_s i_{sq}(t) + \frac{d}{dt}\Big(L_s i_{sq}(t)\Big) + \omega_s L_s i_{sd}(t) + \omega_s \psi_m \tag{2.15}$$

If the *amplitude invariant* 3 to 2 phase transformation is used, see [12], the torque can be calculated as

$$T = \frac{3}{2} p \left( \psi_{sd} i_{sq} - \psi_{sq} i_{sd} \right) \tag{2.16}$$

with vector notation this becomes

$$T = \frac{3}{2} p \, \vec{\psi}_s^{\,dq} \times \vec{i}_s^{\,dq} \tag{2.17}$$

In the application in question, the so called *quadrature current control* is used. This means that $i_{sd} \equiv 0$. Generally, for machines with surface mounted

magnets, the rotor has no saliency, so $L_{sd} = L_{sq} = L_s$. Then quadrature current control gives the maximum torque per unit stator current, see [11]. The torque equation now become simple, as the torque only is depending on $i_{sq}$ and $\psi_m$.

$$T = \frac{3}{2} p \psi_m i_{sq} = K_T i_{rms} \tag{2.18}$$

$K_T$ is the *torque constant* and $i_{rms}$ is the root mean square value of the stator line current. The value of the torque constant is only relevant when quadrature current control is applied, i.e. $i_{sd} = 0$. As $K_T$ is proportional to the magnet flux-linkage, $\psi_m$, a change in the magnets remanence directly affects $K_T$. The required stator voltage modulus $|u_s|$ is calculated as

$$|u_s| = \sqrt{u_{sd}^2 + u_{sq}^2} \tag{2.19}$$

At no load, $i_{sq} = 0$, the stator voltage is

$$|u_s| = \omega_s \psi_m \tag{2.20}$$

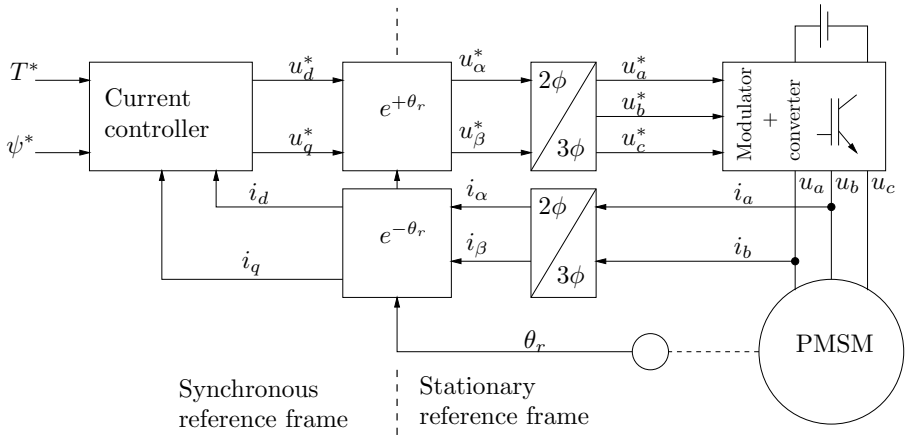


**Figure 2.6** A current controller in a synchronous frame.

A block diagram of a synchronous reference frame controller is shown in figure 2.6. A coordinate transformation has to be made to obtain the current values in the synchronous reference frame and the voltage references in the stationary reference frame.

PI-controllers can be utilised in the $d$- and $q$-directions. Different pole placement strategies for the controllers can be used, for example *predictive deadbeat control*, see [12], or *internal model control*, see [11]. *Direct Flux Linkage Control*, *DFLC*, has been proposed for PMSM control, see [9].

If the concept of vector control is modified, there is the possibility of full or partly table based control, see [4], [7] and [3]. In [3] an identification of the ripple components is described. [19] suggests an adaptive approach to reduce the torque ripple.

If the torque ripple can be reduced by the proper control algorithm, there will be the possibility of allowing a certain amount of torque ripple when designing the machine, thus likely to yield a machine either smaller or cheaper, producing the same average torque, while the drive in an application, produces little or no torque ripple.

## 2.6 Separation of losses

A permanent magnet synchronous machine with surface mounted magnets has a low stator inductance. This is due to the low permeability of modern high energy magnets, which makes the equivalent airgap large. As the stator inductance is low, the stator current have little influence on the stator flux. If the flux is not affected by the current, the flux is also independent of the torque.

If it is possible to assume that the flux in the machine is constant and independent of the current, the iron losses will also be independent of the current and the torque, and only depending on the speed. The copper losses will of course only be depending on the current (torque) and independent of the speed. As a result armature reaction can be neglected, as the flux is constant, and therefore the relationship between torque and current can also be assumed linear.

As the copper losses are proportional to the square of the current, the copper losses are proportional to the square of the torque, so a root mean square torque can be used to calculate the copper losses.

The iron losses will likewise only be depending on flux level and speed, and if the iron losses are assumed to depend on the square of the speed, the iron losses will be proportional to the root mean square value of the speed.

With these assumptions, the losses are depending on the root mean square values of the speed and the torque of a drive-cycle, and not on the maximum torque and speed.

It is important to recognise that with this decoupling of the losses, a machine with nominal torque of $T_{rms}$ at a nominal speed of $n_{rms}$ can perform the task. Such a machine is smaller than a machine which is rated at $T_{max}$ and $n_{max}$.

## 2.7 Torque quality

Torque quality means exact torque, regardless of rotor position, operating point and temperature. This implies negligible cogging torque and torque ripple, as well as constant torque constant, $K_T$.

The torque constant can vary due to armature reaction and variation in magnet flux due to temperature. Armature reaction from the torque producing current might cause saturation, which reduces the magnet flux, and thus reduces the torque to current ratio. To avoid this, the stator inductance should either be low, in order for the flux produced by the stator current to be small compared to the magnet flux, or the stator should be designed to cope with the additional flux without saturation.

If a material with a low temperature coefficient is chosen for the magnets the magnet flux will vary little with temperature, and thus there will be little variation of $K_T$.

Here, cogging torque denotes the zero mean varying torque at no current. It is caused by the stator slotting interacting with the magnets. It is usually remedied by skewing the stator or the magnets, or by shifting the magnet poles. The choice of magnet angle also affects the cogging torque as well as the use of a fractional slot winding. Here, torque ripple denotes the variation of instant torque when the machine is producing average torque, and is caused by the magnets interacting with the stator winding distribution and the stator slotting. It is remedied by distributing or short-pitching the winding, by utilising a fractional slot winding, by skewing the stator or the magnets , or by shifting the magnet poles. These measures aim to attenuate the harmonics of the flux-linkage variation with rotor angle. Of course the cogging also contributes to the torque ripple. An excellent review of the different techniques to reduce cogging and torque ripple is [17]. A favourable quality of the PMSM is that the measures to reduce torque ripple also reduces the cogging, see [17]. It is also possible to reduce cogging and torque ripple by modifying the current waveform, see [4] and [7]. In [17] the conclusion is drawn that it is preferable to reduce the cogging and torque ripple by improving the machine design, rather than using control-based techniques.

## 2.8 Magnets

Today, there are mainly four types of magnet materials available: Neodym-Iron-Bor ($NdFeB$), Samarium-Cobalt ($SmCo$), Aluminium-Nickel-Cobalt ($AlNiCo$) and Ferrite. The typical BH-characteristics *at room temperature* of the materials in their sintered grades are shown in figure 2.7. There are a number of different grades of each of these magnet materials, depending on their composition and manufacturing method. For servo motors in the application considered here, the choice stands between the high energy materials $NdFeB$ and $SmCo$ in their anisotropic sintered grades. $NdFeB$-magnets are

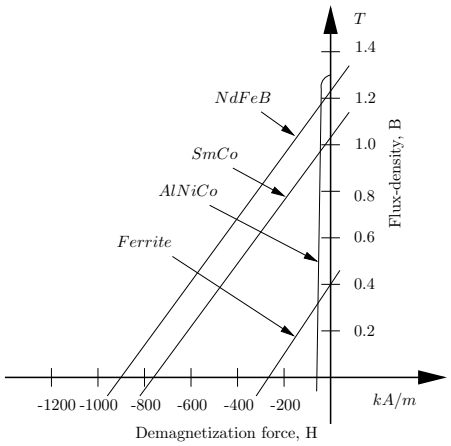


**Figure 2.7** BH-characteristics for the most common magnet materials *at room temperature* in their sintered grades.

generally cheaper than $SmCo$-magnets and have higher remanence at room temperature. $NdFeB$ do however have a larger temperature dependency in both remanence and coercitivity, and lower allowed working temperature compared to $SmCo$. For magnets in the motors considered here it is important to have a high maximum working temperature. It is also important that the temperature dependence is small, as a variation in the remanence (and coercitivity) gives a variation in the flux, and thus in the torque. The major reason for choosing $SmCo$-magnets is the low temperature dependence. Further information on permanent magnets, their manufacturing and properties, can be found in [15].

## 2.9 The present design

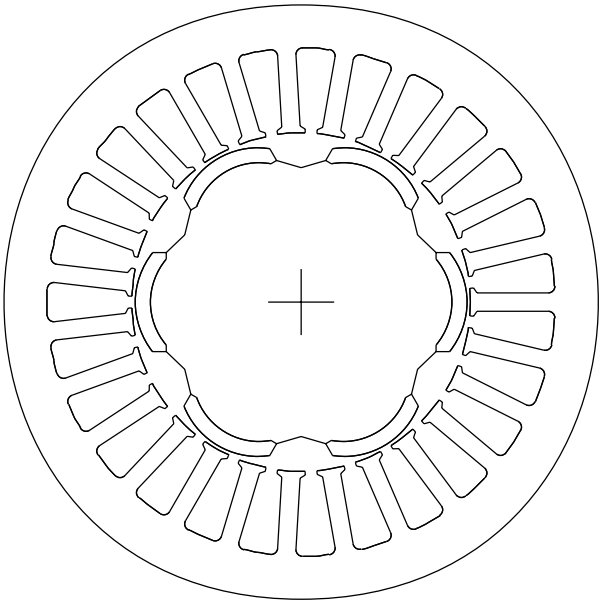

**Figure 2.8** The crossection of the original design.

The present design is a six-pole permanent magnet synchronous machine with surface mounted magnets, see figure 2.8. The active length is 131 mm, the active diameter is 90 mm and the machine has a nominal torque of 5.7 Nm and a nominal speed of 3300 rpm. The rotor is solid, which implies a relatively high inertia. The stator is made by laminations of the steel quality *M300-35A* (Former designation *CK37*). The laminations are 0.35 mm thick. The magnets are of $Sm_2Co_{17}$-type and have a quite complicated crossection, with both the top and the bottom surfaces bent with a radius shorter than the rotor outer radius, see figure 2.8. This is to obtain a more sinusoidal flux-density distribution in the airgap. Appendix A contains data for the magnet material. The stator has 27 slots, so the machine has a fractional slot winding with 1.5 slots per pole per phase. The stator is also skewed one slot pitch, which together with the winding distribution gives the machine a winding factor, $k_w$, of 0.926. This, combined with the magnet shape, contributes to a very smooth torque. The machine is flange mounted, lacks cooling fins and has no fan cooling. The main application of the machine in question is in industrial robots.

# 3

# The design model

## 3.1 Concepts of a new machine

The new machine should have a tube rotor and either rectangular or tapered magnets, see figure 3.1 and 3.2, and a supporting shaft in the centre. The

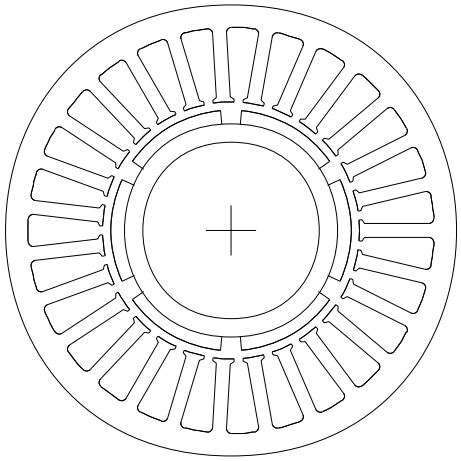

**Figure 3.1** The concept of a new machine with rectangular magnets and a tube rotor.

benefit of a tube rotor is that the iron of the rotor is placed where it is needed the most, to conduct the flux the shortest path between two magnets. The inertia is reduced as the iron volume is reduced, but as the inertia is determined most of all by the material at the periphery of the rotor, the

reduction of inertia becomes less than the reduction of material. The inertia, $J$, of a tube or a pipe with density $\rho$, length $l$, inner radius $r_1$ and outer radius $r_2$ can be calculated as

$$J = \rho\, l\pi \frac{\left(r_2^4 - r_1^4\right)}{2} \tag{3.1}$$

The magnets are mounted on the surface of the rotor, and are therefore determining the inertia to a large extent. Of the same reason, the supporting shaft does not contribute significantly to the inertia of the rotor.

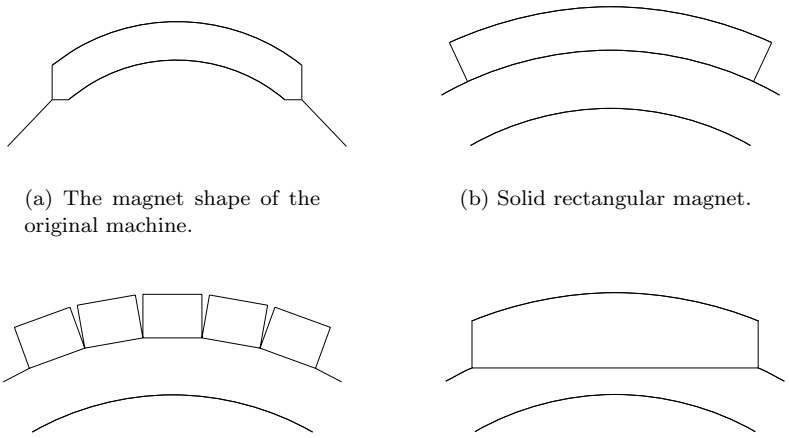

(a) The magnet shape of the original machine.

(b) Solid rectangular magnet.

(c) Rectangular magnet pole consisting of several smaller magnets.

(d) Tapered magnet.

**Figure 3.2** Different magnet shapes.

Rectangular magnets can be manufactured in one piece or assembled from smaller pieces, see figure 3.2(b) and 3.2(c). Tapered shaped magnets are most suited for manufacturing in one piece, see figure 3.2(d). In machines with low pole numbers they give a more sinusoidal flux-density distribution, as the magnets are thicker, giving a higher flux-density, in the middle. Care has to be taken when designing the magnets though, so that the magnet height at the edges will be sufficiently high to avoid danger of demagnetization. For higher pole numbers, the difference between rectangular and tapered magnets vanish.

As the calculations of the performance of a machine are simplified using rectangular magnets, the design model and the equations presented below are for a machine equipped with rectangular magnets.

The winding is allowed to be either distributed or concentrated, and the stator will not be skewed. In the new machine a higher torque ripple will be tolerated, as it is assumed that this can be compensated for by the drive electronics.

## 3.2 Program environment

A procedure in MATLAB has been written that calculates the performance of the machine. Input to the routine is a vector with variables describing the geometry of the machine. The output of the procedure is the object function (material cost) and the constraints. This function is used by MATLABs function for non-linear constrained optimization using sequential quadratic programming. There are upper and lower bounds on the optimization variables. The material properties are constants in the procedure.

## 3.3 The sequence of the calculations

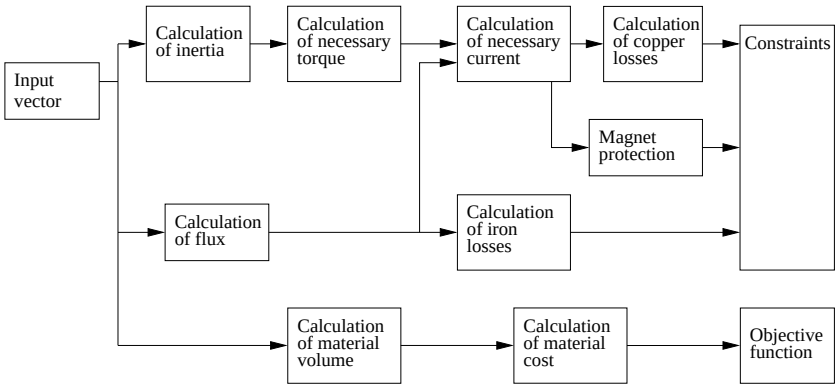


**Figure 3.3** The sequence of the calculations.

As the optimization strategy is to minimize the cost of a machine capable of giving a desired torque during a specified drive cycle, the calculations of the performance of a specific design has to start with a calculation of the inertia

of the design, as it determines the torque that the machine has to supply during the drive cycle. Figure 3.3 shows the sequence of the calculations and their dependence. The calculations are explained in section 3.5 to 3.14, and section 3.15 contains comments on the calculations.

## 3.4 Parametrization of the geometry

The following dimensions describe the machine, see figure 3.4:

$l_{stack}$ The active length of the machine.

$r_{sy}$ The outer radius of the stator.

$r_{si}$ The inner radius of the stator.

$g$ The airgap.

$h_m$ The magnet height.

$h_{ry}$ The rotor yoke height.

$\alpha_m$ The magnet angle.

$h_{tt}$ Height of the shoulders of the teeth.

The rest of the dimensions can be derived from these above. As the purpose of the optimization is to obtain a geometry that has the same outer diameter as the present machine, the outer diameter is fixed and not varied during the optimization. It could easily be included in the optimization, though. A re-parameterization is made to obtain design variables that are better suited for the optimization routine. The design variable vector $\underline{x}$, consists of elements according to table 3.1.

The actual dimensions of the geometry described by the design variables are calculated with equations 3.2 to 3.8.

$$l_{stack} = l_{stack-ref}\,\underline{x}(1) \tag{3.2}$$

$l_{stack-ref}$ is the reference length, set equal to the length of the present design.

$$r_{si} = r_{sy}\underline{x}(2) \tag{3.3}$$

The stator outer radius, $r_{sy}$, is constant, equal to the radius of the present machine, and therefore not included in the design variable vector.

$$h_{sy} = (r_{sy} - r_{si})\,\underline{x}(3) \tag{3.4}$$

$$w_t = \left(\frac{2\pi}{Q} r_{si} - w_{so}\right)\underline{x}(4) \tag{3.5}$$

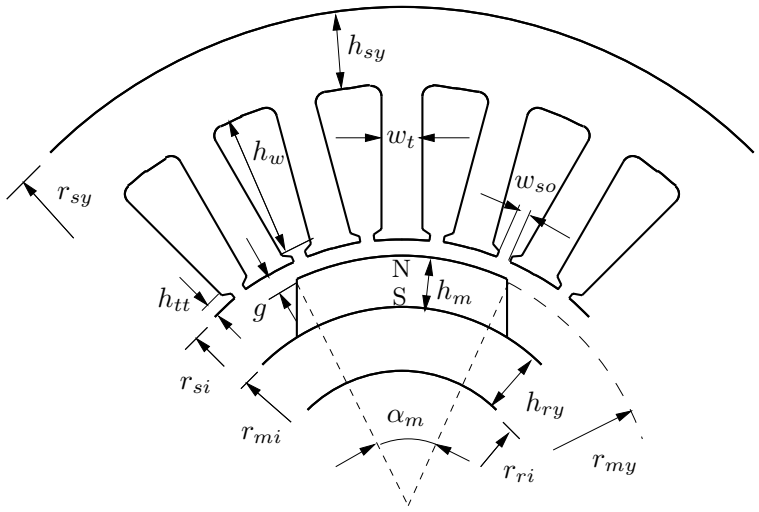


**Figure 3.4** The dimensions of the machine. $l_{stack}$ is the active length of the machine.

$w_{so}$ is the slot opening width, which is set to a constant minimum value, and $Q$ is the number of slots.

$$h_m = (r_{si} - g - r_{shaft})\,\underline{x}(5) \tag{3.6}$$

$g$ is the airgap and $r_{shaft}$ is the radius of the shaft. Both are constant during the optimization.

$$h_{ry} = (r_{si} - g - h_m - r_{shaft})\,\underline{x}(6) \tag{3.7}$$

$$\alpha_m = \frac{\pi}{p}\underline{x}(7) \tag{3.8}$$

## 3.5 Calculation of flux

The no load flux is calculated with a simplified magnetic equivalent circuit (MEC) according to figure 3.5. The flux densities in the machine are assumed to vary as described in [13]. The rotor is assumed to have rectangular magnets, and the flux densities in the stator are assumed to vary according to figure 3.6. In the rotor iron, the flux-density is assumed to vary similarly as

| Design variable | Lower bound | Upper bound | Description |
|---|---|---|---|
| $\underline{x}(1)$ | 0.1 | 10 | Relative length |
| $\underline{x}(2)$ | 0.1 | 0.8 | Relative inner stator radius |
| $\underline{x}(3)$ | 0.1 | 0.9 | Relative stator yoke height |
| $\underline{x}(4)$ | 0.001 | 0.95 | Relative stator tooth width |
| $\underline{x}(5)$ | 0.01 | 0.3 | Relative magnet height |
| $\underline{x}(6)$ | 0.05 | 0.90 | Relative rotor core thickness |
| $\underline{x}(7)$ | 0.2 | 0.95 | Relative magnet angle |

**Table 3.1** The design variables.

in the stator yoke, see figure 3.7. The flux-density in the magnets is assumed to be uniform. The no load flux is calculated in an iterative fashion with the *secant*-method, see [16]. The secant method uses successive function evaluations to find a zero-crossing of a function. The derivative of the function is approximated by a straight line between two function values. At first an initial guess of the flux-density in the magnets, equal to the flux obtained if the iron would be infinitely permeable, is made. A second guess equal to half the first guess. A certain flux-density-level in the magnets produce a corresponding flux-density-level in the different parts in the machine, according to figures 3.6, 3.7 and 3.8.

The flux-density in the airgap, $B_g$, is set to the same value as the flux-density in the magnet, $B_m$, above the magnets and zero in between. The flux-density distribution in the airgap is thus assumed rectangular. The maximum flux-density in a stator tooth, $\hat{B}_t$, in a tooth above a magnet is calculated as

$$\hat{B}_t = \frac{r_{si} 2\pi}{w_t \, Q} B_m; \tag{3.9}$$

$\hat{B}_t$ is thus equal to $B_m$ scaled with the ratio of the tooth width, $w_t$, and the slot pitch, $\frac{2\pi}{Q}$.

The maximum flux-density in the stator yoke, $\hat{B}_{sy}$, is calculated in a similar way. $B_{sy}$ is equal to $B_m$ scaled with the ratio of the stator yoke height, $h_{sy}$, and the magnet width, $\alpha_m r_{si}$.

$$\hat{B}_{sy} = \frac{\alpha_m r_{si}}{h_{sy}} B_m \tag{3.10}$$

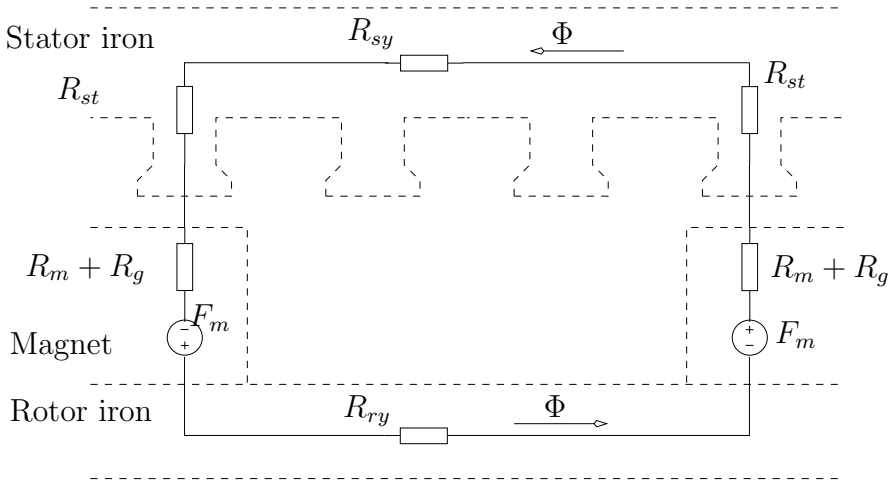


**Figure 3.5** The magnetic equivalent circuit for calculating the no load flux.

The maximum flux-density in the rotor yoke, $\hat{B}_{ry}$, is calculated in the same way.

$$\hat{B}_{ry} = \frac{\alpha_m r_{si}}{h_{ry}} B_m \tag{3.11}$$

The MMF-drop around the flux-path in the MEC is then calculated and compared to the MMF in the magnets, $F_m$, and depending on if the MMF-drop is larger or smaller than the MMF in the magnets, a new estimate of the flux is made. The following condition is sought:

$$\sum_{i=1}^{k} F_i = \sum F_m \tag{3.12}$$

The MMF-drop in the magnets and the airgap are straight forward to calculate, as the materials are magnetically linear. For the MMF-drop calculation of the iron parts, the magnetic field strength as a function of the flux-density, $H(B)$, is tabled. As the stator teeth has uniform thickness, the MMF-drop in a tooth is simply the magnetic field strength multiplied with the length of the tooth.

$$F_{tooth} \quad = \quad H(B_{tooth}) l_{tooth} \tag{3.13}$$

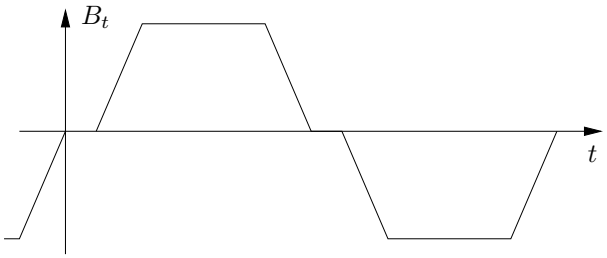


(a) Flux-density variation with time in a stator tooth.

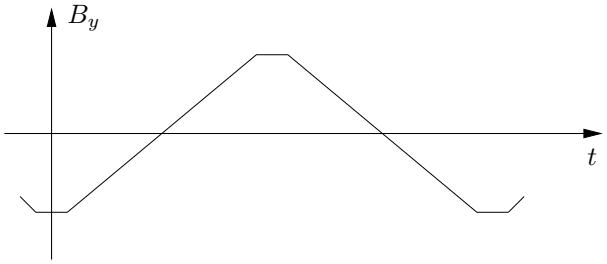


(b) Flux-density variation with time in the stator yoke.

**Figure 3.6** Flux-density variation with time in the stator.

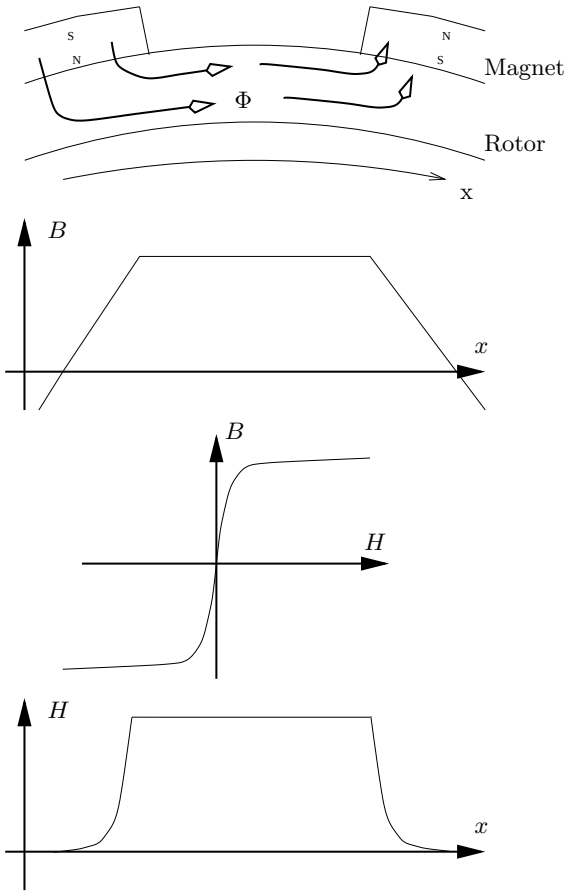


**Figure 3.7** The assumed variation of flux, flux-density and magnetic field-strength between two poles in the rotor.

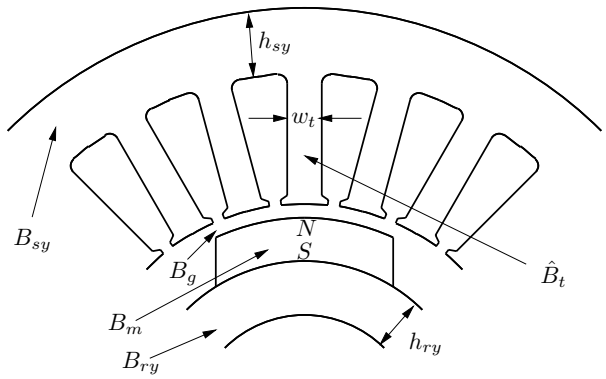


**Figure 3.8** The parts of the machine where the flux density is evaluated.

For the stator and rotor yokes, it is a bit more complicated. The flux-density in the stator and rotor yokes are assumed to vary in the tangential direction according to figure 3.7. For the part of the stator and the rotor that are between two magnets the flux-density is uniform. Therefore the MMF-drop in that part is, in the same way as for the stator tooth, the field strength multiplied with the length of the flux-path between two magnets. For the parts covered by the magnets, numerical integration has to be performed to obtain the MMF-drop, see [8], as the flux-density varies between zero and the maximum value in the yoke. For seven equidistant points on the positive slope of the flux-density curve the magnetic field strength is evaluated, and then Simpsons formula, see [16], is used to obtain the integral.

$$F_{yoke} = \int_l H_{yoke}(l)\ dl \tag{3.14}$$

This way of including the non-linearities of a machine in the model is much simpler than presented in [18]. Only the no load flux is calculated, which means that the effect of the contribution to the stator flux of the stator current is neglected. The benefit of this simpler circuit is that it is very easy to change the pole and the slot number in the calculations.

For the calculation of the torque, the peak value of the fundamental component of the airgap flux, $\hat{B}_{g1}$, is utilised, see figure 3.9. The fundamental is

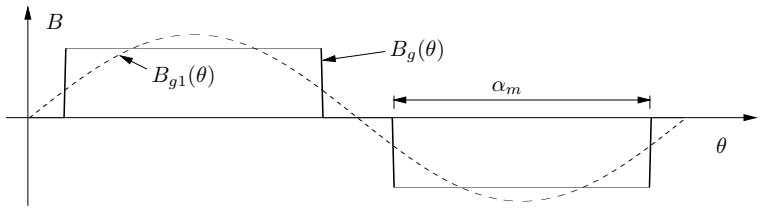


**Figure 3.9** The distribution of the magnet flux in the airgap, $B_g(\theta)$, and its fundamental component, $B_{g1}(\theta)$. $\alpha_m$ is the magnet angle.

calculated as

$$\hat{B}_{g1} = \frac{4}{\pi} \sin\left(p\frac{\alpha_m}{2}\right) B_m \tag{3.15}$$

## 3.6 Calculation of inertia

To be able to calculate the required torque during a drive cycle, the inertia of the rotor must be calculated first. With rectangular magnets, the inertia of the magnets will become

$$J_{mag} = \rho_{mag}\frac{\alpha_{mag}p}{\pi} l_{stack} \frac{r_{my}^4 - r_{mi}^4}{4} \tag{3.16}$$

$\rho_{mag}$ is the density of the magnet material, $\alpha_{mag}$ is the angle of a magnet pole, $p$ is the pole pair number, $l_{stack}$ is the magnetically active length of the machine, $r_{my}$ and $r_{mi}$ are the outer and inner radius of the magnets, see figure 3.10. The inertia of the magnetic part of the rotor, the rotor tube, is calculated according to

$$J_{tube} = \rho_{iron} 2\pi l_{stack} \frac{r_{mi}^4 - r_{ri}^4}{4} \tag{3.17}$$

$\rho_{iron}$ is the density of the iron.

The inertia of the resolver, $J_{resolver}$, the brake, $J_{brake}$, and the first gear stage, $J_{gear-h}$, are specified. The inertia of the part of the shaft extending outside the active part of the stator is included by $J_{shaft-ext}$. The inertia of the shaft in the active part of the stator was calculated as

$$J_{shaft-in} = \rho_{iron} 2\pi l_{stack} \frac{r_{shaft}^4}{4} \tag{3.18}$$

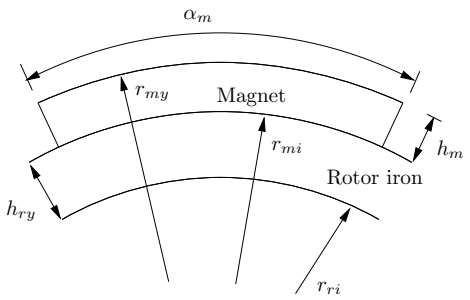


**Figure 3.10** The dimensions of the magnet.

The inertia of the complete rotor could then be calculated as

$$\begin{aligned} J_{rotor} &= J_{mag} + J_{tube} + J_{resolver} + J_{brake} \\ &\quad + J_{shaft-in} + J_{shaft-ext} + J_{gear-h} \end{aligned} \tag{3.19}$$

## 3.7 Calculation of necessary torque

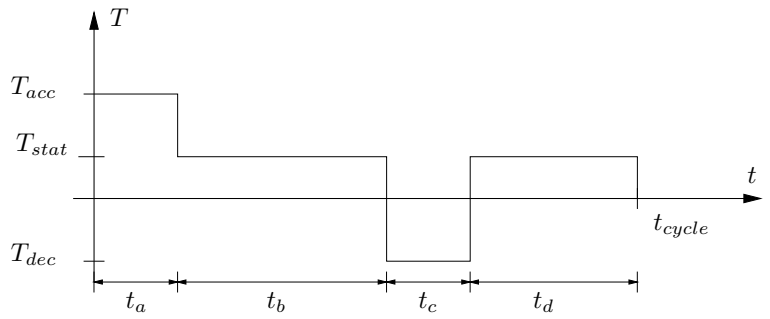


**Figure 3.11** The torque during the drive cycle.

To be able to calculate the losses for the calculation of the constraints, the required *root mean square* torque during a drive cycle must be calculated. The static torque, $T_{stat}$, the maximum allowed gear torque, $T_{gear}$, the torque caused by the gravitational forces on the robot structure and the load, $T_{mg}$, the friction torques for acceleration, $T_{fric1}$, and braking, $T_{fric2}$, and the equivalent load inertia, $J_{load}$, are specified. The maximum acceleration and

the associated acceleration torque and braking torque can then be calculated with equations 3.20-3.22.

$$\left(\frac{d\omega}{dt}\right)_{max} = \frac{T_{gear} + T_{mg}}{J_{load-eq}} \tag{3.20}$$

$$T_{acc} = T_{gear} + T_{fric1} + J_{motor}\left(\frac{d\omega}{dt}\right)_{max} \tag{3.21}$$

$$T_{dec} = T_{gear} - T_{fric2} + J_{motor}\left(\frac{d\omega}{dt}\right)_{max} \tag{3.22}$$

A root mean square torque for the drive cycle, $T_{rms0}$, is then calculated.

$$T_{rms0} = K_{ar}K_{os}\sqrt{\left(T_{acc}\right)^2\frac{i}{2} + \left(T_{dec}\right)^2\frac{i}{2} + \left(T_{stat}\right)^2(1-i)} \tag{3.23}$$

See figure 3.11. $T_{rms0}$ is calculated with two additional constants, $K_{ar}$ and $K_{os}$. $K_{ar}$ is compensating for that armature reaction is not included in the model, as only the no load flux is calculated. The required torque is increased with 10-20% to give a margin for a possible torque reduction due to saturation caused by armature reaction. $K_{os}$ is a factor which is compensating that the present machine might be slightly over (under) sized, and to get a comparable machine, $T_{rms0}$ is multiplied with $K_{os}$. $K_{os}$ is set to 1 if no such compensation is to be made. $T_{rms0}$ is additionally modified to take thermal considerations into account, see equation 3.36, to obtain the root mean square torque, $T_{rms}$, used in the following calculations.

$$T_{rms} = \underbrace{\frac{1}{K_{cool}}\sqrt{\frac{100}{95}}}_{\substack{\text{Thermal}\\ \text{considerations}\\ \text{see eqn. 3.36}}} K_{ar}K_{os}\sqrt{\left(T_{acc}\right)^2\frac{i}{2} + \left(T_{dec}\right)^2\frac{i}{2} + \left(T_{stat}\right)^2(1-i)} \tag{3.24}$$

The intermittence, $i$, is specified by the drive cycle. It is assumed that the time for acceleration, $t_a$, is equal to the time for braking to standstill, $t_c$. $i$ is calculated according to equation 2.4.

## 3.8 Calculation of necessary current

Utilizing the concept of a linear current density at the inner periphery of the stator, see [8], the torque, $T$, is calculated according to

$$T = \pi r_{si}^2 l_{stack}\hat{A}_1\hat{B}_{g1} \tag{3.25}$$

$r_{si}$ is the stator inner periphery, $l_{stack}$ is the magnetically active length of the machine, $\hat{A}$ is the peak value of the fundamental of the linear current density, and $\hat{B}$ is the peak value of the fundamental of the flux density in the airgap. It is here assumed that quadrature current control is used, i.e. that the linear current density and the flux density in the airgap are in phase. The necessary peak value of the linear current density for the root mean square torque, $T_{rms}$, is then calculated

$$\hat{A} = \frac{T_{rms}}{\pi r_{si}^2 l_{stack} \hat{B}_{g1}} \tag{3.26}$$

From the linear current density the peak value of the ampere-turns value for a phase, $N\hat{I}$, is calculated, see [8].

$$N\hat{I} = \frac{3}{\pi} \frac{r_{si}}{p\, k_w} \hat{A} \tag{3.27}$$

The root mean square value of the slot current (total current in a slot) is then simply calculated as

$$NI_{slot-RMS} = \frac{1}{q} \frac{N\hat{I}}{\sqrt{2}} \tag{3.28}$$

$q$ is the number of slots per pole per phase.

## 3.9 Calculation of copper losses

The copper length of half a coil is

$$\frac{l_{coil}}{2} = l_{stack} + l_{ec} \tag{3.29}$$

where $l_{stack}$ is the active length of the machine and $l_{ec}$ is the length of the end-turns. $l_{ec}$ is calculated as

$$l_{ec} = \sigma_{lec} \frac{\pi}{p} (r_{sy} - h_{sy}) \tag{3.30}$$

$\sigma_{lec}$ is an empirical factor, see [13], which is set to 1.6. The current density, $j_{cu}$ in the copper is

$$j_{cu} = \frac{NI_{slot-RMS}}{A_{slot} k_{fcu}} \tag{3.31}$$

$A_{slot}$ is the slot cross-sectional area, and $k_{fcu}$ is the copper fill factor. The copper volume is then

$$V_{cu} = A_{slot} k_{fcu} \frac{l_{coil}}{2} s \tag{3.32}$$

as the number of slots is $s$. The total copper losses for a certain root mean square torque will then be

$$P_{cu} = \rho_{cu} j_{cu}^2 V_{cu} \tag{3.33}$$

## 3.10 Calculation of iron losses

The derivation of the equations for the iron losses is made in appendix B. The following formula is obtained

$$\begin{aligned} P_{fe} &= \rho_{fe} k_{ffe} V_{sy} \left( \frac{8 C_e p \omega_{rms}^2 \hat{B}_{sy}^2}{\pi \alpha_m} + C_h \hat{B}_{sy}^{n(\hat{B}_{sy})} \overline{\omega} \right) \\ &+ \rho_{fe} k_{ffe} V_{st} \left( \frac{2}{\pi^2} C_e \, p \, Q \omega_{rms}^2 \hat{B}_{st}^2 + C_h \hat{B}_{st}^{n(\hat{B}_{st})} \overline{\omega} \right) \end{aligned} \tag{3.34}$$

$\rho_{fe}$ is the density of the laminated iron, $k_{ffe}$ is the iron fill or stacking factor, $V_{sy}$ is the volume of the stator yoke and $V_{st}$ is the volume of the stator teeth. $\hat{B}_{sy}$ is the peak flux density in the stator yoke and $\hat{B}_{st}$ is the peak flux density in the stator teeth. $C_e$ and $C_h$ are the loss coefficients for the eddy current and the hysteresis losses respectively. $\omega_{rms}$ is the root mean square mechanical speed and $\overline{\omega}$ the mean mechanical speed. $\alpha_m$ is the magnet angle.

## 3.11 Thermal considerations

The specification of the motor manufacturer states that the machine should be able to run the specified drive cycle with a maximum of a $100°C$ average temperature rise in the windings. The constraint for the maximum losses was set to

$$\sqrt{P_{cu} \left( P_{cu} + P_{fe} \right)} \quad < \quad \Delta T_{max} \frac{\sqrt{l_{stack}}}{C_{therm}} \tag{3.35}$$

See appendix D. $\Delta T_{max}$ is the maximum allowed temperature rise, here $100°C$.

Additional thermal considerations are made. In addition to the motor manufacturers specification above, the robot manufacturer specifies that the average temperature of the windings of the motors should not rise more than $95°C$ compared to the ambient. As the cooling situation in the robot varies from robot type to robot type, as well as from robot axis to robot axis, for each axis a cooling factor is specified, which states the cooling situation for the motor compared to the standard test, see section 6.1. The root mean square torque is then modified:

$$T_{rms} = \frac{T_{rms0}}{K_{cool}} \sqrt{\frac{100}{95}} \tag{3.36}$$

$K_{cool}$ accounts for the cooling situation, and $\sqrt{\frac{100}{95}}$ is compensating for the difference in the winding temperature specifications. According to the previous assumptions, the copper losses are proportional to the square of the torque, and neglecting the iron losses, $P_{fe}$, in equation 3.35, the temperature rise will be proportional to the copper losses. Increasing the torque requirements by $\sqrt{\frac{100}{95}}$ will then represent a 5 % lower temperature in the machine. To be consistent with the robot manufacturers way of calculating $T_{rms}$, the difference in temperature specifications is included according to above, instead of altering $\Delta T_{max}$ in equation 3.35 to $95°C$.

## 3.12 Magnet protection

The minimum tolerable magnet height considering the risk of demagnetization, $h_{m-min}$, is calculated with equation 3.37, see appendix C.

$$h_{m-min} = \frac{K_{demag} N\hat{I} + B_{m-min}\frac{g}{\mu_0}}{H_c - \frac{B_{m-min}}{\mu_r \mu_0}} \tag{3.37}$$

$N\hat{I}$ is the maximum peak phase current at normal operation, i.e. corresponding to the current at acceleration. $K_{demag}$ is the demagnetization safety factor, i.e. the relation between the maximum current at normal operation and the current at which the magnets will get (partially) demagnetized if the current vector is aligned with the negative $d$-direction. $B_{m-min}$ is the minimum tolerable flux-density in the magnets due to risk of demagnetization.

## 3.13 Calculation of the constraints

The constraints are the relations that must not be violated, for example geometrical constraints like:

- The rotor outer radius plus the airgap must not be larger than the stator inner radius
- The magnet angle times the number of poles must not be larger than $2\pi$

Other constraints are the demagnetization and thermal constraints described above. It is common practise to describe a constraint as an expression that should be less than zero.

$$g(x) < 0 \tag{3.38}$$

It is often possible, by a change in variables or re-parametrization, to include the constraints in the upper and lower boundaries of the input variables. This has partly been done here, most of the geometrical constraints have become redundant by the choice of variables. Some still remain, and these are preventing that the minimum width of the stator yoke, $h_{sy-min}$, the minimum width of the stator teeth, $w_{t-min}$, and the minimum height of the stator slots, $h_{w-min}$, are violated. These constraints are expressed as

$$h_{sy-min} - h_{sy} < 0 \tag{3.39}$$
$$h_{w-min} - h_w < 0 \tag{3.40}$$
$$w_{t-min} - w_t < 0 \tag{3.41}$$

The next constraint is the minimum magnet height:

$$h_{m-min} - h_m < 0 \tag{3.42}$$

See appendix C for the calculation of the minimum magnet height, $h_{m-min}$.

The cooling capability constraints the total losses:

$$\frac{C_{therm}}{\sqrt{l_{stack}}}\sqrt{P_{cu}\left(P_{cu}+P_{fe}\right)} - \Delta T_{max} < 0 \tag{3.43}$$

See appendix D for the calculation of the thermal constraints. Finally, the rotor yoke thickness is constrained, due to mechanical reasons, it must not be thinner than a minimum value, $h_{ry-min}$.

$$h_{ry-min} - h_{ry} < 0 \tag{3.44}$$

## 3.14 Calculation of the material cost

The object function of the optimization is the material cost of the machine. The cost is obtained as material volume times density times price per mass for each of the respective materials. The total magnet volume, $V_{mag}$, is:

$$V_{mag} = 2p\alpha_m \frac{r_{my}^2 - r_{mi}^2}{2} \tag{3.45}$$

The copper volume is calculated according to

$$V_{cu} = qA_{slot}k_{fcu}\big(l_{stack} + l_{ec}\big) \tag{3.46}$$

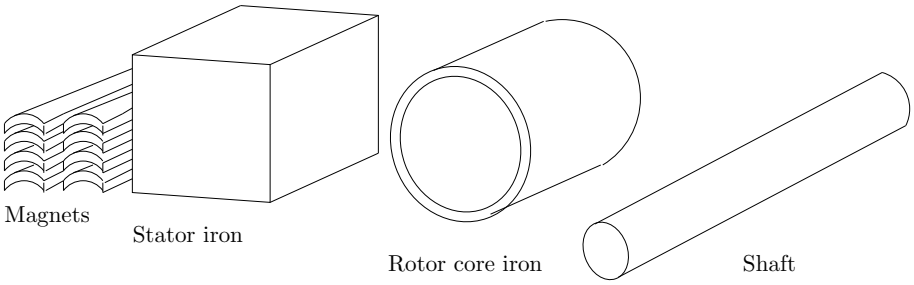


**Figure 3.12** The material for the calculation of the material price.

The iron volume is calculated as material consumed by the stator laminations and the iron volume of the shaft. The stator iron volume is calculated as the active length times a square area with the sides equal to the stator outer diameter. This is approximately the material consumed by the stator, as the material inside the stator inner radius will be of no use. It is also difficult to place the stampings to close to each other when the laminations are punched. The rotor core consumes material equal to the volume of a cylinder with length $l_{stack}$ and the inner and outer diameter of the rotor core. The shaft consumes material equal to the shaft length times the shaft radius squared. The iron volume will then be

$$V_{fe} = l_{stack}(2r_{sy})^2 + l_{stack}\pi(r_{mi}^2 - r_{ri}^2) + l_{shaft}\pi r_{shaft}^2 \tag{3.47}$$

$l_{shaft}$ is the length of the shaft, which is the length of the shaft of the old machine minus the active length of the old machine plus the active length of

the new machine, $l_{stack}$. The shaft thus extends equally beyond the stator stack on both machines. The price of the material for the machine will be:

$$Price_{tot} = C_{mag}\rho_{mag}V_{mag} + C_{cu}\rho_{cu}V_{cu} + C_{fe}\rho_{fe}V_{fe} \tag{3.48}$$

$C_{mag}$, $C_{cu}$ and $C_{fe}$ are the price per weight for the magnet material, copper and iron respectively.

## 3.15 Comments on the design model

### Program environment

The design model is implemented as a function in MATLAB, but can be implemented in any programming language, for example Pascal, C or Fortran77. MATLAB is slower than an implementation in for example C, but very convenient, as there is no need for declaration of variables and a number of procedures and functions are readily available, for example functions for plotting and optimization.

### The sequence of the calculations

The sequence of the calculations determines to quite an extent what can be calculated by the function. The calculation of the nominal torque of a given geometry would require a reformulation of the expressions for torque, current etc. The formulas by themselves can be put together separately though, and be used for calculation of any arbitrary quality of a machine.

### Parametrization of the geometry

The parametrization of the geometry presented here is very well suited for optimization, as most geometric constraints have been obsolete as geometric infeasible combinations of the design variables are prevented by the upper and lower boundaries of the design variables. The drawback is that the true dimensions are not explicitly expressed by the design variables, but has to be calculated from them. This will cause extra work if the performance of a geometry with specified dimensions, for example the stator yoke height and teeth width, should be calculated.

### Calculation of flux

When calculating the flux, there is always a tradeoff between model complexity and computing time. The classical way of dealing with the nonlinear

permeability of the iron is to assume that the iron is infinitely permeable and that all the MMF is consumed in the airgap. To avoid that the optimization yields a design with infinitely small tooth and stator yoke width, a maximum flux density in the iron is introduced as a constraint. The maximum flux density is the choice of the designer. This kind of model is easy to implement, as it is merely a sequence of formulas, similar (in most cases identical) to those presented in this chapter.

A more complex model is the *Magnetic Equivalent Circuit* (MEC), see [18]. The model consists of an arbitrary number of linear and non-linear reluctances, and the accuracy, complexity and computing time are determined by the number of elements.

The most accurate (and time consuming) method is the *Finite Element Method*, see [8]. Usually, even if an analytical or magnetic equivalent circuit model is used for the optimisation of an electric machine, the results are checked by FEM. Ideally FEM should be used for the optimization directly, but it has up until now been regarded as too time consuming.

The model presented here is a very simple MEC-model. There is only one flux to determine, and therefore the solving of the flux is fast with the secant-method, and no derivatives of reluctances has to be supplied. The secant-method estimates the derivative by the two last function evaluations. As the model calculates the MMF-drop in the stator and rotor yokes by integrating the magnetic field strength over half the magnet angle, a reluctance derivative with respect to flux for the stator and rotor yokes would have to be obtained by taking differences.

In the model, it is also easy to change the pole and the slot number. In the optimization, the optimal flux-density in the stator teeth and yoke and in the rotor yoke is determined along with the geometry, so they do not have to be chosen by the designer. In the same way, the optimal tradeoff between rotor yoke thickness (flux-density) and inertia can be made by the optimization routine.

### Calculation of necessary torque

The calculation of the necessary torque has a lot of safety, thermal and compensation factors, which of course all could be included into one. It is beneficial though, to have control over what compensates what and to what degree, and that is best done by a factor for each requirement. The torque calculation can easily be extended for a more complicated drive cycle, with for example a number of different torque levels during acceleration and braking.

Torque linearity is not considered in the model, and no measures are taken to assure that the assumption of no armature reaction is violated. This has

to be checked separately by FEM.

### Calculation of iron losses

The loss formula for the iron, equation B.1, includes a part for the hysteresis losses, $C_h \hat{B}^{n(\hat{B})}\omega$. This is inconsistent with the concept of a root mean square torque, where the iron losses are assumed to be proportional to $\omega_m^2$. Instead, a coefficient for the total iron losses, $C_{fe}$, should be introduced and fit to the loss curves for the magnetic steel for a loss formula of the form

$$\frac{P_{fe}}{M_{fe}} = C_{fe}\hat{B}^2\omega^2 \tag{3.49}$$

The formula for the iron loss, equation 3.34, can then be used with $C_e$ exchanged to $C_{fe}$, and the hysteresis loss part dropped.

### Thermal considerations

Equation 3.43 is not valid for a general machine. It merely states how the temperature rise varies with the copper and iron losses for a certain machine. It was however feasible to use here, as the new machine would have the same outer diameter and approximately the same length as the present machine. The $\sqrt{l_{stack}}$-term in the expression for the temperature rise is uncertain, as only three machines provided data for the estimation of the relationship *permissible losses-length*.

### Calculation of the material cost

The costs for machine housing, endshields, bearings and other mechanical parts are assumed constant, independent of the dimensions of the magnetic circuit. Also, the cost of machining and labour are assumed independent of the dimensions of the machine, so the optimization only minimizes the material cost. Again, this is due to that the new machine would have a size and design concept similar to the present. No investigation have been made of the eventual cost benefits of the tapered magnet shape and the tube-rotor concepts.

# 4

# Optimization

## 4.1 Optimization strategy

### Choice of object function

When optimizing an electric motor, there are multiple choices of the object function available. The object function is the specific property of the machine to optimized, for example torque, volume or cost. Of course a 'good' motor is desired, but what is a 'good' motor and what to do when the different goals are contradicting? A good motor has low price, high torque density and high torque quality, but unfortunately, these goals are contradicting. In a PM-machine, the torque density can always be improved, though sometimes just marginally, by adding more magnet material. So the best machine with respect to torque density would be the one which has the rotor consisting of magnets only. Such a machine would be very expensive, and is therefore of course not the optimum, even if it could appear to be so by just focusing on the torque density. Focusing on torque quality would yield a machine with with very low torque, as all the measures to obtain a ripple free and smooth torque such as distributing the winding, skewing of the stator, shaping of the magnets etc., reduces the average torque. Focusing on the price will give a machine with high volume for a given torque, with as little magnet material as possible, as the magnet material is the most expensive material in the machine. It is doubtful if such a machine is desired, even if the expression 'maximum torque per unit price' seems very popular. There is also the question of what should be the object function and what should be the constraints. There is the possibility of obtaining the goals above by letting one of them be the object function, or the property to be optimized, and then incorporate the others as constraints.

One could for example choose the torque as the object function and put constraints as the maximum material cost and maximum torque ripple. One could also choose the material cost as the object function, i.e. minimize the cost, and use constraints as a minimum rated torque and a maximum torque ripple.

Here, we choose to minimize the material cost of a machine, capable of performing a specific task. This means that we have the demands of a drive cycle for a specific axis in the robot, we start with a too large and expensive machine, and then we try to minimize the material cost by reducing size, changing proportions etc. while still being able to perform the specified task with the machine, i.e. run it according to the drive cycle without overheating.

**Optimization objective:**

*Minimize the material cost of a machine capable of performing a specific task*

### Choice of optimization algorithm

The optimization of an electric machine is a constrained non-linear optimization problem. One approach, see [14], is to make an analytical model of the machine, and then test all possible combinations of a set of parameters describing the machine and its performance. The best combination of the parameters is taken as the optimum. The parameters are varied in steps, and the smaller the steps the better the accuracy and the longer the computing time, there is a tradeoff between accuracy and computing time. The benefit of this approach is that the true global minimum is found. The drawback is that the model has to be simple or the number of parameters to be varied has to be kept low, to ensure reasonable computing times. This probably rules out more complicated models, like *Magnetic Equivalent Circuit*-models (MEC), see [18]. It certainly rules out models based on the *Finite Element Method* (FEM).

Another approach is to convert the constrained optimization problem to an unconstrained problem and augmenting the object function with barrier functions, preventing the constraints to be violated. This has the advantage that

efficient search methods can be used during the optimization, which saves computing time. Therefore, MEC and FEM models can be used. The drawback of this method is that if the optimum is near or on a constraint, the optimization problem might become ill-conditioned, see [1]. This might imply long computing time or convergence to a point different from the optimum. The optimum found might be a local optimum as no guarantee is given for convergence to the global optimum.

Here the approach is to use a method for constrained optimization, utilizing *Sequential Quadratic Programming*. No transformation of the constraints is made. The algorithm uses the gradients of the object function and the constraints to find feasible search directions and an optimum. There is no guarantee, however, that the algorithm converges to the global optimum. As there are no demands for efficiency, it is likely that the optimum will be on the thermal constraint of the model, and then it is natural to use a method which can inherently cope with constraints. More information about optimization is to be found in [1].

### Input and output variables

A function for calculating the performance of a servo motor has been written in the computing environment MATLAB , see chapter 3. The function calculates the material cost of a machine with its dimensions determined by a set of input parameters. The function also calculates maximum tolerable losses and minimum allowed magnet height, and these values are, together with some minimum dimensions, used as constraints in the optimization. For the optimization, the MATLAB-routine **constr** has been used, which sequentially calls the function above with varied parameters to find a design with minimum material cost which does not violate the constraints.

The MATLAB-optimisation routine **constr** uses *Sequential Quadratic Programming* to minimize a function $f(\underline{x})$, where $\underline{x}$ is a vector with the design parameters, under the condition that the constraints, $\boldsymbol{g}(\underline{x}) < 0$, must not be violated. Both $f$ and $\boldsymbol{g}$ are functions of the design variable vector. The vector $\underline{x}$ is iteratively modified to obtain a minimum in the object function, $f(\underline{x})$, without violating the constraints.

The constraints prevent the optimization routine to converge to an infeasible design, for example with a larger rotor diameter than the stator inner diameter, with too thin teeth or magnets, or with too high losses. By modifying the choice of design parameters, most geometric constraints can be incorporated in the upper and lower bounds of the design parameters. Here the design parameters expresses not the real dimensions of a machine, but the dimensions relative the other dimensions or a reference dimension. Thus, the

design parameters, with one exception, varies between 0 and 1.

### Optimization sequence

The sequence of the optimization was according to figure 4.1. First the optimization routine was run with different pole and slot numbers to determine the most favourable combination. Only integer-slot designs were considered. The optimization, however, yielded a design with too high torque ripple.

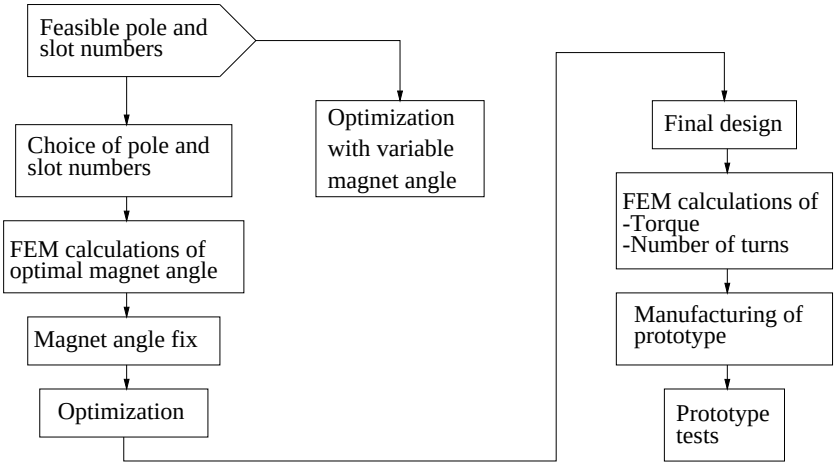


**Figure 4.1** The sequence of the optimization.

Therefore, the magnet angle which would give the minimum torque ripple was investigated by FEM. Then the optimization was rerun with this magnet angle, and some additional changes to the dimensions to incorporate the tolerance of the dimensions. FEM was then again used for checking the average torque, the torque ripple, and to calculate the number of turns in the stator winding. This was then followed by prototype manufacturing and tests.

## 4.2 Parameters for the optimization

### Drive cycle

The requirements of the drive cycle for axis 5 of *IRB4400* are according to table 4.1.

| | | | | | |
|---|---|---|---|---|---|
| $n_{max}$ | : 3300 | $rpm$ | $J_{brake}$ | : 1.00 | $kg\,cm^2$ |
| $n_{rms}$ | : 1650 | $rpm$ | $i$ | : 0.10 | |
| $T_{gear}$ | : 6.15 | $Nm$ | $K_{cool}$ | : 1.0 | |
| $T_{fric1}$ | : 2.55 | $Nm$ | $K_{ar}$ | : 1.10 | |
| $T_{fric2}$ | : 0.4 | $Nm$ | $K_{os}$ | : 1.12 | |
| $T_{stat}$ | : 3.39 | $Nm$ | $K_{demag}$ | : 3.8 | |
| $J_{load}$ | : 14.70 | $kg\,cm^2$ | | | |
| $J_{gear-h}$ | : 0.56 | $kg\,cm^2$ | | | |
| $J_{resolver}$ | : 0.12 | $kg\,cm^2$ | | | |

**Table 4.1** The requirements of the drive cycle.

### Dimensions

The outer diameter was fixed to $90\,mm$, the same diameter as the present machine. This to obtain a machine of comparable size.

The airgap was also kept to the same value, $0.5\,mm$.

### Magnets

The magnet material and grade was kept the same as the magnet material in the present machine, $Sm_2Co_{17}$ of grade **S3/225**, see appendix A. $NdFeB$-materials were not considered.

### Iron material

The magnetic steel for the stator laminations was kept the same as for the present machine, i.e. the steel quality *M300-35A*, 0.35 mm thick. For the rotor tube the standard construction steel *SS1650* was chosen.

### Material cost

The cost of the three materials considered in the optimization is given in table 4.2. The values are given in *per unit* values.

### Fill factors

The iron fill factor, $k_{ffe}$, was set to 0.98. The copper fill factor, $k_{fcu}$, was set to 0.42. This was far too optimistic, an reasonable value should be 0.33. Due to this error, the optimized machine should have substantially higher copper losses than calculated, and therefore the nominal torque should be lower than calculated.

| | | |
|---|---|---|
| Iron | : | 1.0 *p.u* |
| Copper | : | 3.5 *p.u* |
| Magnet | : | 250.0 *p.u* |

**Table 4.2** The material cost.

## 4.3 Comparison of pole numbers

| Number of slots/pole/phase | Number of poles | | | |
|---|---|---|---|---|
| | $2p = 4$ | $2p = 6$ | $2p = 8$ | $2p = 10$ |
| $q = 1.0$ | $Q = 12$ | $Q = 18$ | $Q = 24$ | $Q = 30$ |
| $q = 1.5$ | $Q = 18$ | $Q = 27$ | X | X |
| $q = 2.0$ | $Q = 24$ | X | X | X |
| $q = 2.5$ | $Q = 30$ | X | X | X |

**Table 4.3** The investigated combinations of pole numbers, $2p$, and slot numbers, $Q$. $q$ is the number of slots/pole/phase. Slot numbers higher than 30 has not been regarded as feasible for a machine of this size, and combinations yielding $Q > 30$ are marked with $X$ in the table.

In the initial stage different pole numbers and different winding arrangements were investigated. The maximum number of slots was assumed to be 30 for a machine with an outer diameter of 90 mm, and pole numbers from four to ten were examined with the optimization routine, with slot and pole numbers according to table 4.3. Only integer slot designs were considered. The geometry in the optimization was without any skew, and the magnet angle was a parameter. Cogging and torque ripple were neglected at this stage, and as a consequence, machines with distributed windings and a winding factor below unity performed less than their counterparts with concentrated windings and a unity-winding factor. If torque quality had been considered the designs with distributed windings would yield better relative results, as such a winding is more 'sinusoidally' distributed and therefore produces less torque ripple. Neither was the improved thermal properties of a machine with a higher number of slots included.

This optimization is a minimization of the material cost of a machine which can perform a specific task, and the algorithm is terminated when the change in price for a change in the variables is lower than a specified tolerance.

| $2p$ | $Q$ | $q$ | $k_w$ | $l_{stack}$ $[mm]$ | $r_{si}$ $[mm]$ | $\alpha_m$ $[^\circ_{mec}]$ | $h_m$ $[mm]$ | $J$ $[kgcm^2]$ | $Cost$ $[pu]$ |
|---|---|---|---|---|---|---|---|---|---|
| 4 | 12 | 1 | 1.0 | 119 | 45.2 | 48.3 | 3.3 | 3.15 | 71.1 |
| 4 | 18 | 1.5 | 0.9452 | 130 | 45.1 | 47.9 | 3.3 | 3.34 | 77.0 |
| 4 | 24 | 2 | 0.9659 | 127 | 45.9 | 47.0 | 3.4 | 3.42 | 78.0 |
| 4 | 30 | 2.5 | 0.9567 | 138 | 50.4 | 43.9 | 3.5 | 4.73 | 87.0 |
| 6 | 18 | 1 | 1.0 | 97 | 41.2 | 35.4 | 2.7 | 2.01 | 54.0 |
| 6 | 27 | 1.5 | 0.9452 | 105 | 48.2 | 33.7 | 2.7 | 3.06 | 61.1 |
| 8 | 24 | 1 | 1.0 | 89 | 45.1 | 27.5 | 2.2 | 2.14 | 46.0 |
| 10 | 30 | 1 | 1.0 | 89 | 52.4 | 22.1 | 1.7 | 2.85 | 41.6 |

**Table 4.4** Result of the optimization for different values of $p$ and $q$. $p$ - pole pair number, $Q$ - number of slots, $q$ - number of slots per pole per phase, $k_w$ - winding factor, $l_{stack}$ - active length, $r_{si}$ - stator inner radius, $\alpha_m$ - magnet angle (mechanical angle), $h_m$ - magnet height, $J$ - inertia, $Cost$ - material cost.

Therefore optimization of designs with just slightly different pole numbers or number of slots/pole/phase can yield quite significant different dimensions, as different dimensions can yield similar prices. It seems clear, however, that a higher pole number yields a lower price. An advantage of a multiple pole machine is that the magnets are exposed to a smaller demagnetizing MMF for the same current loading compared to a machine with a lower pole number. This means that the magnets can be made thinner, so the magnet volume decreases. As magnets are the most expensive part of the machine, this is a very important aspect. The rotor yoke also can be made thinner for a machine with higher pole number, which implies lower inertia, and thus less need for torque for a specified acceleration. A smaller and cheaper machine can thus perform the desired task.

*It was decided to build a 10-pole machine with $Q = 30$ and $q = 1$.*

## 4.4 Torque ripple calculations by FEM

A finite element calculation of the torque at nominal load indicated that a 10-pole design with an arbitrary magnet angle could have a very high torque ripple, almost 50% peak-to-average. To obtain a design with more moderate ripple, the torque ripple for different magnet angles were calculated.

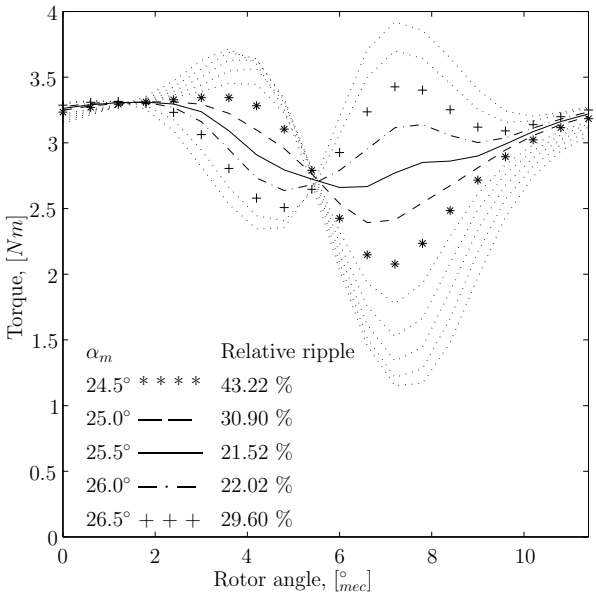


**Figure 4.2** The torque ripple for different magnet angles with 30% of nominal current for a 10-pole machine with $Q = 30$, $q = 1$ and no skew.

Magnet angles from $22.0^\circ_{mec}$ to $27.5^\circ_{mec}$ in steps of $0.5^\circ_{mec}$ were investigated, see table 4.5, and the relative torque ripple, $\Delta T$, was calculated.

$$\Delta T = \frac{T_{max} - T_{min}}{\overline{T}} \tag{4.1}$$

$T_{max}$ is the maximum instantaneous torque, $T_{min}$ is the minimum instantaneous torque, and $\overline{T}$ is the average torque. The calculations were made over an interval of $60^\circ_{el}$ which is $12^\circ_{mec}$ for this 10-pole machine. The calculations were made with 30% of maximum current, to avoid saturation effects.

It was found that a magnet angle of $25.5^\circ_{mec}$ would give the lowest relative torque ripple.

## 4.5 Optimization of ten-pole design

The optimization routine was run again with the magnet angle fixed to $25.5^\circ_{mec}$. The data of the resulting machine from that optimization is shown

| Magnet angle | Relative ripple |
|---|---|
| $22.0^\circ_{mec}$ | 95.30 % |
| $22.5^\circ_{mec}$ | 90.32 % |
| $23.0^\circ_{mec}$ | 82.12 % |
| $23.5^\circ_{mec}$ | 71.83 % |
| $24.0^\circ_{mec}$ | 58.15 % |
| $24.5^\circ_{mec}$ | 43.22 % |

| Magnet angle | Relative ripple |
|---|---|
| $25.0^\circ_{mec}$ | 30.90 % |
| $25.5^\circ_{mec}$ | 21.52 % |
| $26.0^\circ_{mec}$ | 22.02 % |
| $26.5^\circ_{mec}$ | 29.60 % |
| $27.0^\circ_{mec}$ | 41.11 % |
| $27.5^\circ_{mec}$ | 49.52 % |

**Table 4.5** The relative torque ripple for different magnet angles.

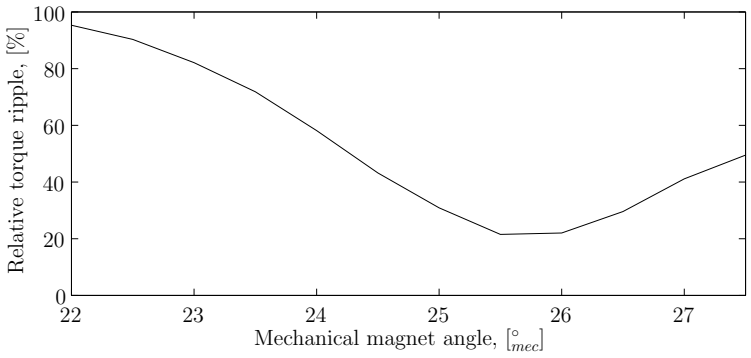


**Figure 4.3** The relative torque ripple for different magnet angles with 30% of nominal current for a 10-pole machine with $Q = 30$, $q = 1$.

in table 4.6

As the original machine has a stator inner diameter, $2r_{si}$, of 51.26 $mm$ which is almost the same as for the optimized geometry, the manufacturer of the machine requested that the prototype should have the same inner diameter as the present machine for manufacturing reasons. A new optimization was run with the stator inner diameter fixed to 51.26 $mm$. In addition to this, the airgap was increased with 0.15 $mm$ to 0.65 $mm$ in the optimization, to account for a 'worst case' of stator and rotor dimensions within the manufacturing tolerances (maximum airgap, minimum magnet height etc.). The result is shown in table 4.7.

The copper losses, $P_{cu}$, and the iron losses, $P_{fe}$, calculated for the final design,

| $2p$ | $Q$ | $q$ | $k_w$ | $l_{stack}$ $[mm]$ | $2r_{si}$ $[mm]$ | $\alpha_m$ $[^\circ_{mec}]$ | $h_m$ $[mm]$ | $J$ $[kgcm^2]$ | $Cost$ $[pu]$ |
|---|---|---|---|---|---|---|---|---|---|
| 10 | 30 | 1 | 1.0 | 81 | 52.6 | 25.5 | 1.7 | 2.94 | 41.8 |

**Table 4.6** Result of the optimization with a 10-pole machine with a magnet angle of $25.5^\circ_{mec}$.

| $2p$ | $Q$ | $q$ | $k_w$ | $l_{stack}$ $[mm]$ | $2r_{si}$ $[mm]$ | $\alpha_m$ $[^\circ_{mec}]$ | $h_m$ $[mm]$ | $J$ $[kgcm^2]$ | $Cost$ $[pu]$ |
|---|---|---|---|---|---|---|---|---|---|
| 10 | 30 | 1 | 1.0 | 85 | 51.26 | 25.5 | 1.75 | 2.58 | 44.0 |

**Table 4.7** Result of the final optimization with a 10-pole machine with a magnet angle of $25.5^\circ_{mec}$ and stator inner diameter of $51.26\,mm$.

are shown in table 4.8. No calculation of friction and windage losses were made.

| Copper losses, $P_{cu}$ | Iron losses, $P_{fe}$ |
|---|---|
| 86.9 W | 46.2 W |

**Table 4.8** The calculated iron and copper losses for the final design.

## 4.6 Comparison of the designs

A comparison of the three designs is made in table 4.9. It can be noted that the difference in cost between having the magnet angle free or fixed, i.e. a high or a lower torque ripple, is very small. The difference in price when the airgap is increased is bigger.

## 4.7 Magnet shape

It was decided to use tapered magnets, see figure 3.2(d). As the pole number is 10, the difference between tapered magnets and rectangular magnets, see figure 3.2(b), for which the optimization is made, is small. The transition from rectangular to tapered magnets adds magnet material and increases the flux, and thus gives an additional safety margin to compensate for the difference between the model and reality.

The final design was now according to figure 4.4.

| $l_{stack}$ $[mm]$ | $2r_{si}$ $[mm]$ | $r_{si}$ free | $\alpha_m$ $[^\circ_{mec}]$ | $\alpha_m$ free | $h_m$ $[mm]$ | $g$ $[mm]$ | $J$ $[kgcm^2]$ | $Cost$ $[pu]$ |
|---|---|---|---|---|---|---|---|---|
| 89 | 52.4 | yes | 22.1 | yes | 1.7 | 0.5 | 2.85 | 41.6 |
| 81 | 52.6 | yes | 25.5 | no | 1.7 | 0.5 | 2.94 | 41.8 |
| 85 | 51.26 | no | 25.5 | no | 1.75 | 0.65 | 2.58 | 44.0 |

**Table 4.9** Comparison of the three designs, with $\alpha_m$ free/fixed and $r_{si}$ free/fixed. All designs have $2p = 10$, $Q = 30$, $q = 1$ and $k_w = 1$.

## 4.8 FEM calculations on final design

The finite element method (FEM) was used for some final calculations on the optimized design according to figure 4.4. FEM was used for the calculation of the number of turns in the stator winding. Calculations of torque and induced voltage were also made with FEM.

### Calculation of $N_s$

The stator voltage is calculated according to equation 2.20. At no load, the current is zero, and therefore the stator voltage is

$$|u_s| \quad = \quad \omega_s \psi_m \tag{4.2}$$

To calculate $\psi_m$, FEM was used. To calculate the flux-linkage for one coil, the following steps are performed:

1. Integrate the *magnetic vector potential per unit length*, $A$, over each of the two coil sides of a coil.
2. Divide by the slot area. In this way, the *average* vector potential in each coil side is obtained.
3. Calculate the difference in average vector potential and multiply by the active length, and thus obtain a *coil flux*, $\phi$
4. Multiply with the pole number, $p$, and the number of turns, $N_s$, to obtain the flux linkage

The formula for the flux linkage is thus

$$\psi \quad = \quad p\left(\frac{N_s}{S_{coil}} l_{stack} \iint A_2 \; ds - \frac{N_s}{S_{coil}} l_{stack} \iint A_1 \; ds\right) = p\phi N_s \tag{4.3}$$

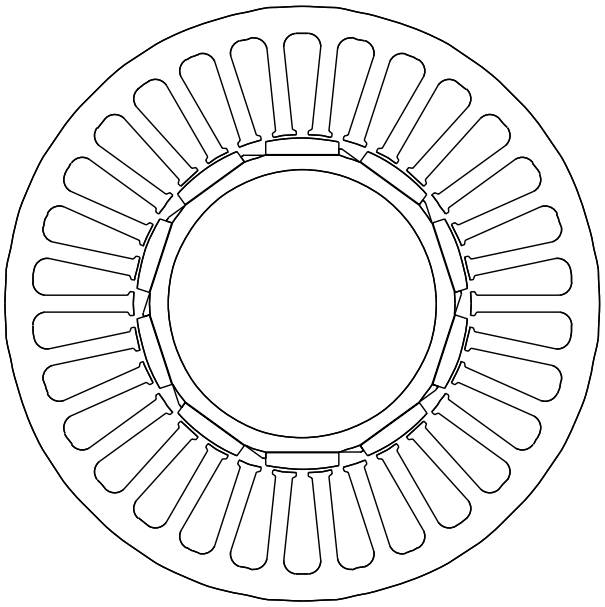

**Figure 4.4** The cross section of the new design.

FEM-calculations were made, modelling only one slot-pitch, according to figure 4.6, for each each $0.6^\circ_{mec}$ over a slot-pitch, $12^\circ_{mec}$ or $60^\circ_{el}$. Unfortunately, a proper function for calculating the integral of the vector potential over an element was not included in the FEM-program used, Ansys5.3. Instead the integral of the vector potential over an element was calculated as the vector potential of some centre point of the element, multiplied with the area of the element. To obtain the integral of the vector potential over a whole slot, the results for all elements of the slot was summed.

As the model only included one slot for each phase, the vector potential for a coil was obtained by multiplying the vector potential in the associated slot with two, with the appropriate sign, this due to the anti-symmetric boundary conditions.

For each rotor angle, the following calculations were performed to obtain the

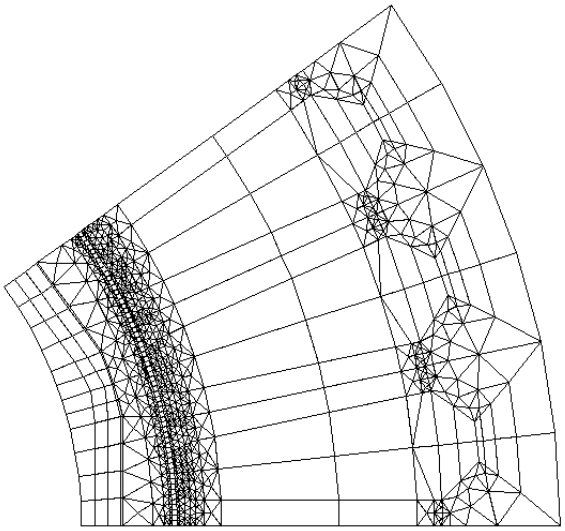

**Figure 4.5** The meshing of the geometry. Note the large number of elements in the airgap.

coil flux for each phase:

$$\phi_a(\theta_r) = \frac{2}{S_{a+}} l_{stack} \iint A_{a+}(\theta_r)\ ds \tag{4.4}$$

$$\phi_b(\theta_r) = \frac{2}{S_{b+}} l_{stack} \iint A_{b+}(\theta_r)\ ds \tag{4.5}$$

$$\phi_c(\theta_r) = -\frac{2}{S_{c-}} l_{stack} \iint A_{c-}(\theta_r)\ ds \tag{4.6}$$

$(\theta_r)$ is the rotor angle. To obtain the coil-flux for $360^\circ_{el}$, the coil-flux for the three phases were added to a vector in a sequence with signs according to equation 4.7

$$\begin{aligned} \phi(\theta_r) = \big[&\phi_a(\theta_r)\,;\, -\phi_b(\theta_r)\,;\, \phi_c(\theta_r)\,; \\ &-\phi_a(\theta_r)\,;\, \phi_b(\theta_r)\,;\, -\phi_c(\theta_r)\big] \end{aligned} \tag{4.7}$$

A plot of the coil-flux variation during a rotation of the rotor of $360^\circ_{el}$ together with its fundamental is shown in figure 4.7. The peak value of the fundamental, $\hat{\phi}_1$, was calculated to $6.6072 \cdot 10^{-4}\ Wb$.

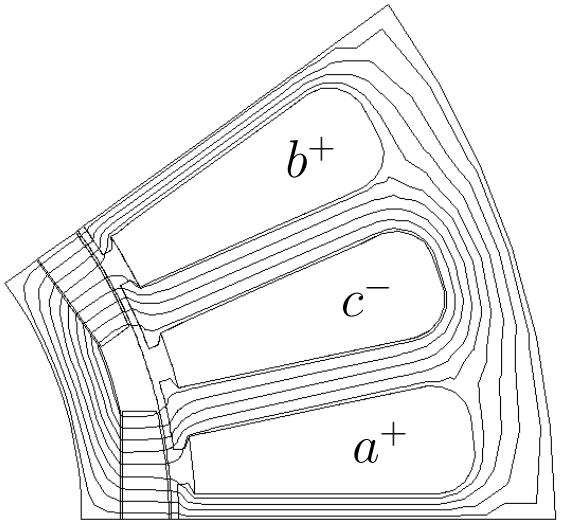


**Figure 4.6** Flux-lines under no load conditions. The vector potential, $A$, is used for the calculation of the number of turns.

The desired induced *phase-to-phase*-voltage was according to the specification $46 \pm 2.3\ V_{RMS}$ at 1000 rpm. This corresponds to a peak phase voltage of

$$\hat{u}_{f1000} \quad = \quad 46\frac{1}{\sqrt{3}}\sqrt{2} = 37.56\ [V] \tag{4.8}$$

The peak phase voltage can also be written

$$\hat{U}_f = \omega_s \psi_m = \omega_s p \hat{\phi}_1 N_s \tag{4.9}$$

$\psi_m$ is the magnet flux-linkage of one phase. The electrical frequency, $\omega_s$, is calculated from the mechanical speed, $n$.

$$\omega_s \quad = \quad p\frac{n}{60}2\pi \tag{4.10}$$

The required number of turns is now

$$\begin{aligned} N_s \quad &= \quad \frac{\hat{U}_{f1000}}{\omega_s p \hat{\phi}_1} = \frac{\hat{U}_{f1000}}{p\frac{n}{60}2\pi p \hat{\phi}_1} = \frac{46\frac{1}{\sqrt{3}}\sqrt{2}}{5\frac{1000}{60}2\pi 5 \cdot 6.6072 \cdot 10^{-4}} \\ &= \quad 21.71 \ \approx \ 22\ [turns] \end{aligned} \tag{4.11}$$

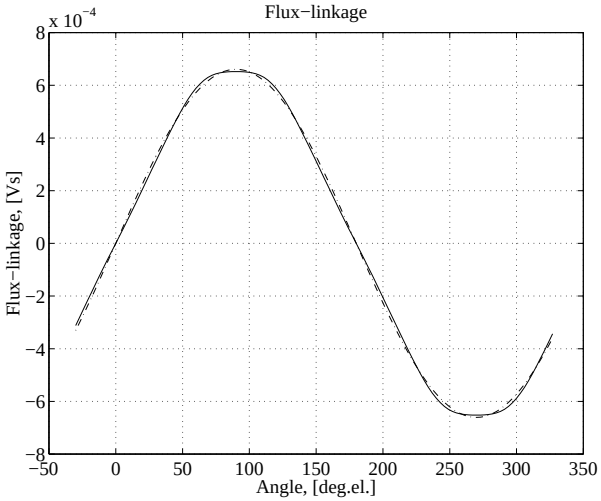


**Figure 4.7** The stator coil flux variation as a function of rotor angle, along with its fundamental.

The voltage waveform with 22 turns in the stator winding at 1650 rpm was calculated according to figure 4.8.

| Harmonic | 1 | 3 | 5 | 7 | 9 | 11 | 13 | 15 | 17 | 19 |
|---|---|---|---|---|---|---|---|---|---|---|
| Fraction [%] | 100.0 | 4.8 | 10.9 | 4.3 | 1.7 | 0.5 | 0.2 | 0.0 | 0.2 | 0.3 |

**Table 4.10** The harmonics relative the fundamental.

The voltage contains a substantial amount of harmonics, see figure 4.9 and table 4.10. However, as the machine is Y-connected, all harmonics that are multiples of three (3, 9, 15 etc.) cancel. Also the harmonics of order 11 and higher are of very small amplitude, and this leaves only the 5:th and the 7:th harmonics as relevant.

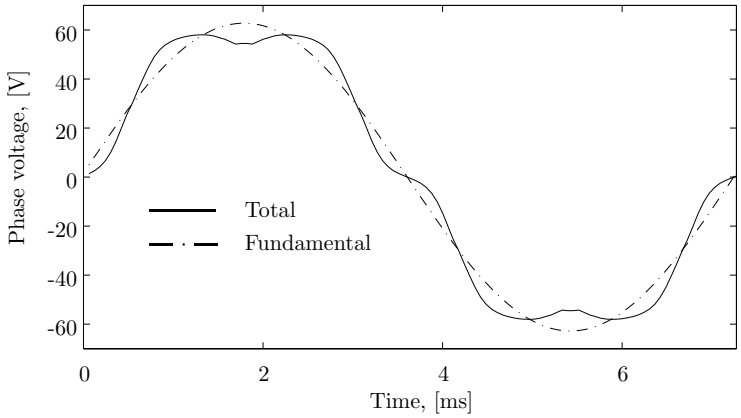


**Figure 4.8** The calculated phase voltage at 1650 rpm, with the fundamental.

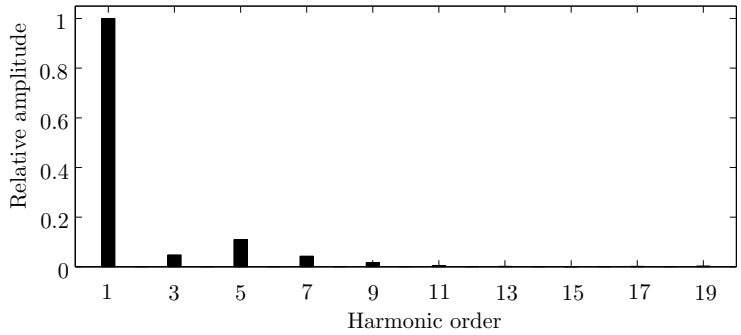


**Figure 4.9** The relative amplitude of the fundamental and the harmonics of the phase voltage.

### Calculation of torque

Calculations of the torque were made by FEM for no current (cogging torque), nominal current and the current for maximum acceleration. The results of the FEM-calculation of the torque is shown in table 4.10 and figure 4.10. The relative torque ripple, $\Delta T$, is quite high, 17.21 % at nominal torque. $\Delta T$ is calculated according to equation 4.1. The margin between the FEM-calculated torque and the corresponding required torque calculated by the optimization routine, is approximately 5 % at maximum torque. The change from rectangular to tapered magnets is likely to be the cause of this increase.

No finite element analysis of the design with rectangular magnets have been made.

| | Nominal current | Maximal current |
|---|---|---|
| NI | 159.31 $A_{rms}$ | 307.03 $A_{rms}$ |
| I | 7.24 $A_{rms}$ | 13.96 $A_{rms}$ |
| $T_{opt}$ | 5.49 Nm | 10.58 Nm |
| $T_{FEM}$ | 5.90 Nm | 11.15 Nm |
| $\Delta T$ | 17.21 % | 15.12 % |
| $T_{FEM} - T_{opt}$ | 0.411 Nm | 0.576 Nm |
| $\frac{T_{FEM}}{T_{opt}}$ | 1.075 | 1.054 |

**Table 4.11** The nominal and maximal currents. The maximal current is the current for maximum acceleration. $T_{opt}$ is the necessary torque according to the optimization, $T_{FEM}$ is the average torque calculated by FEM and $\Delta T$ is the relative torque ripple calculated by FEM.

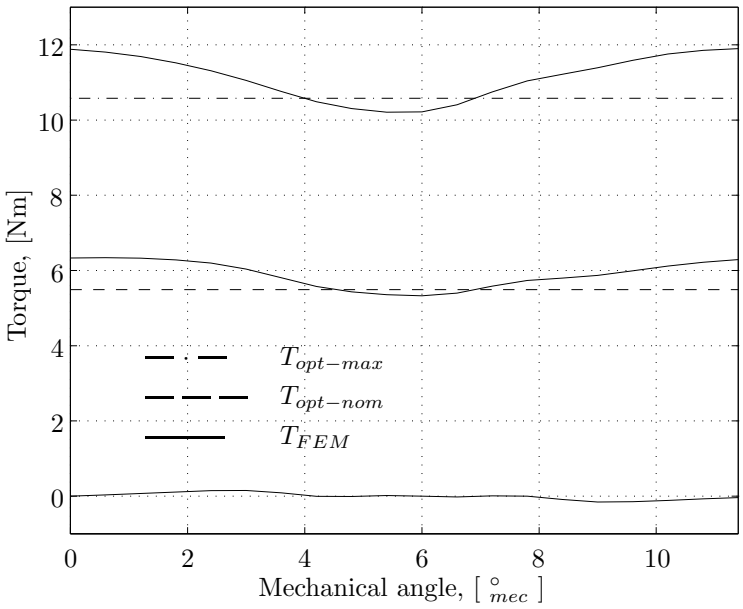


**Figure 4.10** The torque versus rotor angle (electrical angle) for no current, nominal current and maximal current. $T_{opt-max}$ is the maximum and $T_{opt-nom}$ the nominal torques according to the optimization. $T_{FEM}$ is the corresponding values calculated by FEM.

# 5

# The Prototype

## 5.1 The stator

### The housing

The rotor was designed using the housing, the endshields and the bearings of the present machine. The stator housing was shortened due to shorter active length of the new machine.

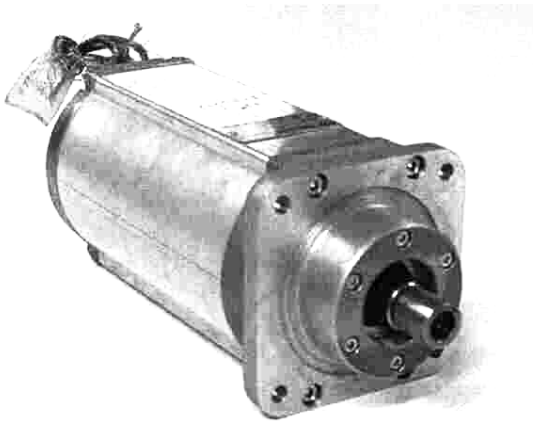

**Figure 5.1** The stator housing.

### Stator laminations

The stator laminations were laser cut from the material *M300-35A*, 0.35 mm.

### Winding

The winding was made from 22 turns with 5 wires in parallel. The wire effective copper diameter was $0.5\,mm$, so this implies a total copper area of $22\,mm^2$. The slot area for the final design was $63\,mm^2$, so the fill factor, $K_{fcu}$, was 34 %. The usual fill factor for the present machine is 31-32 %. There is a large discrepancy between the actual $K_{fcu}$ and the assumed $K_{fcu} = 0.42$. This leads to approximately 24 % higher copper losses for the same current, or 11 % lower current and torque for the same copper losses. The figure 0.42 for the copper fill factor is not unrealistic though, but the lower value is determined by the winding equipment of the manufacturer of the servo motors.

## 5.2 The rotor

### Mechanical design of the rotor

The rotor consists of a shaft, a tube, washers, fasten elements and magnets, see figure 5.2 and 5.3. The washers are fastening the tube on the shaft, and are kept in place by a nut and a spacer.

### The rotor shaft

The shaft was designed according to figure 5.4. The parts outside the active part of the machine was copied from the present design.

### The rotor tube

The rotor tube was machined from a tube in the material *SS1650*. Flat surfaces, for the magnets to be mounted on, were machined, and supports for the magnets were left on one side of the flat surfaces.

### The resolver and the brake

The rotor was fitted with a resolver of the same type as for the present machine. The resolver had two poles and required an excitation frequency of 5 kHz.

The present machine is fitted with a brake, but to ease the testing, the prototype was not fitted with a brake.

**Figure 5.2** The rotor disassembled.

## 5.3 Magnets

### Magnet manufacturing

The magnets were manufactured by Swift Levick Magnets Ltd. in Barlborough, England, and are of grade S3. The magnets are of the tapered type, see figure 5.6. The data for the magnet quality is in appendix A. A magnet pole was divided in six parts, and made up of six magnets. As there were 10 poles, there were 60 magnets all together on the rotor. 75 magnets had been ordered from the manufacturer to allow a few magnets to be broken during the handling.

The magnets were glued to the rotor tube, and then a retaining layer of kevlar fibre was applied around the rotor. The glue only served to keep the magnets in place until the kevlar layer was in place.

With allowance for tolerances, the magnet height was specified to 2.53 mm (the maximum magnet height in the middle of the magnet). The first intention was to have the magnets manufactured with machinery allowance, glue them on the rotor, and then grind them to their final shape on the rotor. As

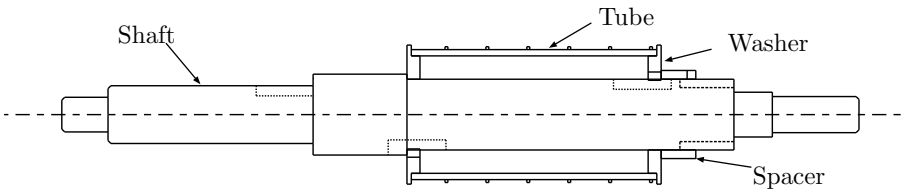


**Figure 5.3** The cross section of the assembled rotor without magnets, seen from the side. The nut fastening the tube and the washers is not included.

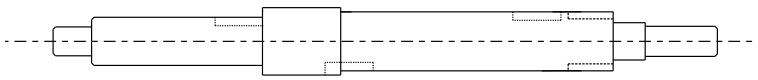

**Figure 5.4** The shaft.

the glue layer is approximately 0.1 mm thick, the intention was to mount two 0.1 mm diameter piano wires under each magnet, to ensure a constant and well defined glue layer.

The magnets were, however, delivered machined to their final shape. Therefore there was no need for grinding, and also the concept of the glue layer defining piano wire was dropped, as it was assumed that its benefit was negligible when no machining after magnet mounting was to be done.

Before the magnets were mounted on the rotor tube, their dimensions and relative flux were measured.

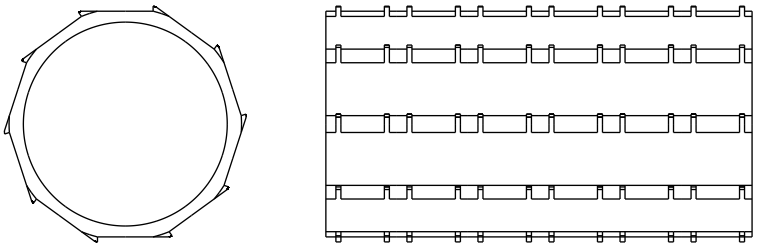

**Figure 5.5** The rotor tube.

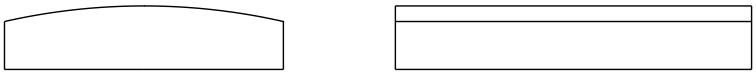

**Figure 5.6** The shape of the magnets. There were 60 magnets mounted on the rotor.

### Magnet dimension measurements

The height was measured for all the magnets, and the result of the measurements are shown in figure 5.7. The point of measurement was in the centre of the magnet, so the maximum height was measured.

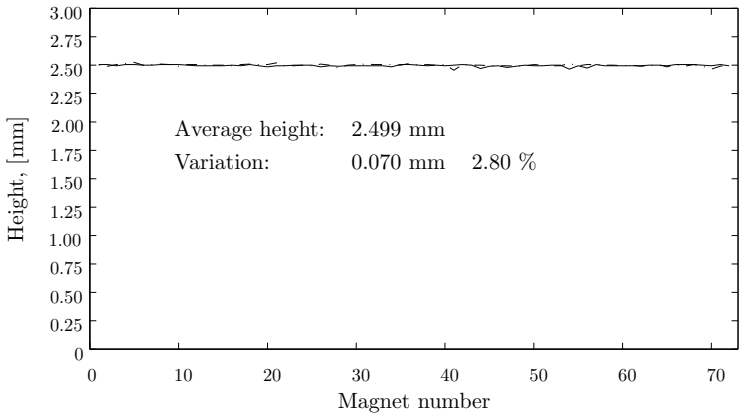


**Figure 5.7** The shape of the magnets. There were 60 magnets mounted on the rotor.

As can be seen in figure 5.7, the variation of magnet height is vary small, only 2.8 %. The variation was calculated as the maximum minus the minimum height, divided by the average. The deviation of the average height from the specified was 0.03 mm, which is well within the specified tolerance of 0.1 mm.

### Magnetic remanence

A relative measurement of the magnets remanence was made in a setup according to figure 5.8.

The setup was made from a screw-vice, used for fastening details to be machined in a upright drill. The actual dimensions were not measured and were thus unknown, and therefore the measurements were relative only. The screw-vice was made of magnetic iron with high permeability, so the magnet

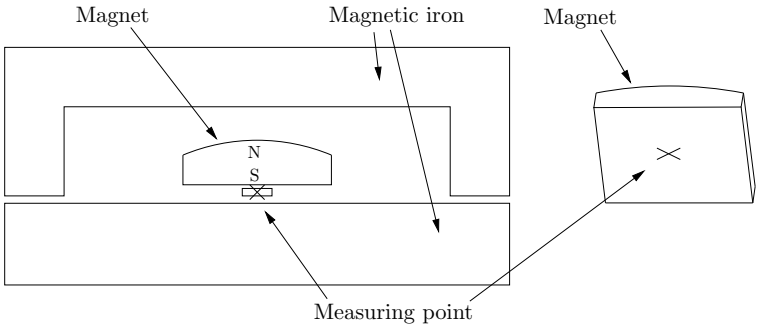


**Figure 5.8** The setup for measuring the magnets.

flux in the measuring setup is determined by the distance between the iron pieces, the magnet height and the remanence of the magnet. The measuring principle was based on the hall-effect, with a probe containing a hall-element connected to an electronics unit with a display. A fixture was made to fix the position of the magnet relative the screw-vice. The fixture also fixed the position of the measuring probe, which was used to measure the flux-density. The point of measurement was below the flat under side, in the middle of the magnet, see figure 5.8.

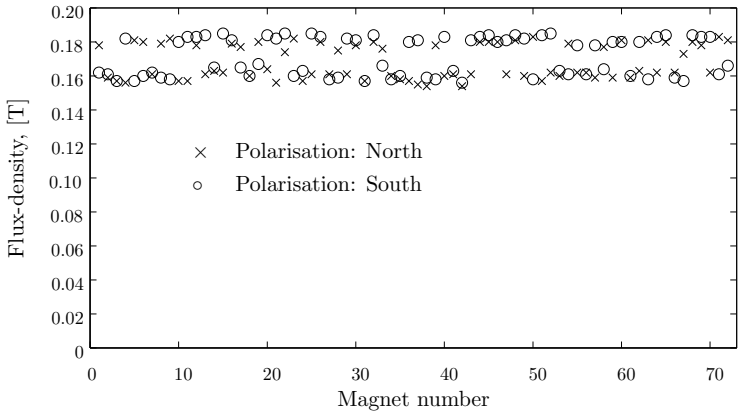


**Figure 5.9** The relative flux density of the magnets.

A diagram of the results of the measurements is shown in figure 5.9. As can be seen in figure 5.9, there seemed to be two different magnet qualities, one with relative flux-density of approximately 0.18 and one with relative flux-density

of approximately 0.16. According to the manufacturer, all magnets were from the same batch, and the difference in flux density could be explained by the grinding of the magnets.

When $Sm_2Co_{17}$-magnets are manufactured, $Sm_2Co_{17}$-powder is first compacted in a press, with the die cushion and the stamp shaped to give the magnet approximately its correct dimensions, see figure 5.10. During the pressing, a magnetic field is applied to magnetically align the grains in the die. With aligned grains, a stronger magnet is obtained, capable of producing more flux. The field is in this case (as usual) applied in the pressing direction. The magnet is then ejected from the die cushion and moved to a furnace with controlled atmosphere, for sintering. After the sintering, the magnet is ground to its final dimensions.

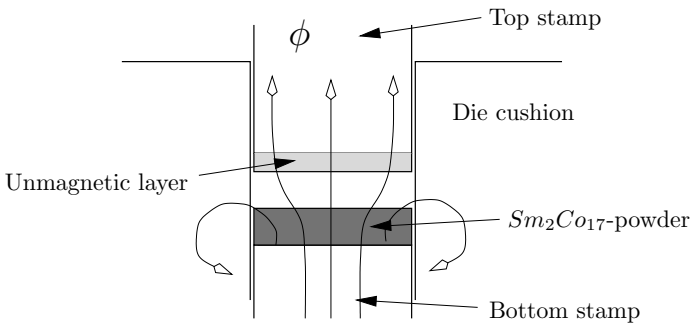


**Figure 5.10** Crossection of the magnet press.

As the magnet is slightly magnetized from the applied field when it is ejected from the die cushion, there is attracting forces between the magnet and the top and bottom stamps. To make sure that the magnet stays on the bottom stamp and is released from the top stamp, the top stamp has a layer of non-magnetic material at the surface, see figure 5.10. This causes the aligning field to be weaker near the top stamp, and prevents the grains near the top stamp to achieve the same level of orientation as the grains near the bottom stamp. Therefore, the magnetic alignment will be lower in the part of the magnet which has been near the top stamp during the pressing.

The magnets of the prototype were pressed to a rectangular crossection, see figure 5.11, it was considered too expensive to manufacture a new dedicated press tool for this prototype. No track was kept of what side of the magnets that had been facing the top stamp during the pressing, so when the magnets were ground to their final shape, approximately half of them had their 'bottom stamp' side ground to a curved shape, and half of them their 'upper

stamp' side.

When the magnets were ground, more material had to be removed to obtain the curved upper side than the flat bottom side. Approximately half the magnets had their stronger, more aligned, 'bottom stamp' side ground to the curved upper side shape, and thus had more magnet material with better alignment removed. These magnets then became weaker than the other half of the magnets, which had, to a higher extent, material from their less aligned 'upper stamp' side removed.

In series production, a dedicated press tool will be manufactured, as it will be too expensive to grind the curved shape from a rectangular block. Then there will be no mixing of the 'upper' and 'bottom' stamp sides, so the strength of the magnets in a batch will not vary to the extreme extent that it did in this case.

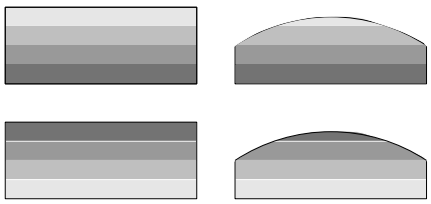

**Figure 5.11** The effect of grinding. The areas with darker shade represent areas with better magnetic alignment of the $Sm_2Co_{17}$-grains.

### Magnet selection

To make all the poles producing the same flux, the magnets were selected so the sum of the measured relative flux density of the magnets in a pole would be equal for all poles. This is really not important with the configuration of the test machine, with a straight stator and the rotor poles not shifted. But if torque ripple would be reduced with either a skewed stator or with having the rotor poles shifted, the 'strength' of the individual poles and magnets becomes important, as these two torque ripple compensation schemes are based on that the torque ripple from different magnets or poles are partially or completely cancelling each other. The result of the selection procedure is in table 5.1. Note how closely the poles are matched, the deviation from the average of all poles is less than 0.7 % for each pole.

If it is assumed that the upper relative value, approximately 0.18, is the normal value of the flux-density, the rotor poles, which have an average relative value of approximately 0.17, could be regarded as made of a material with

| Pole pair: | 1 | 2 | 3 | 4 | 5 |
|---|---|---|---|---|---|
| Polarisation north: | 0.1690 | 0.1690 | 0.1690 | 0.1690 | 0.1690 |
| Polarisation south: | 0.1690 | 0.1690 | 0.1690 | 0.1703 | 0.1702 |

**Table 5.1** The average of the relative flux-density in each pole.

lower remanence. If the magnets in figure 5.9 are split into parts, one with relative flux-density below 0.17, and the other with relative flux-density over 0.17, the upper part will have a mean relative flux-density of 0.1809, see table 5.2. The mean relative flux-density of the magnets of the prototype is 0.1692, so there is a decrease of 6.4 %. In the following FEM-calculations, the magnet material of the prototype was regarded as made of a material with lower remanence, so the remanence, $B_r$, and the coercitive force, $H_c$, were both lowered with 6.4 %.

| Upper mean ($B_{rel} > 0.17$): | 0.1809 |
|---|---|
| Average on prototype: | 0.1692 |
| Decrease: | 6.4 % |

**Table 5.2** Mean relative flux-densities of the magnets of the prototype and the magnets with relative flux-density higher than 0.17. *Upper mean* is the mean relative flux-density of the magnets with relative flux-density higher than 0.17.

### Magnet assembly

The gluing of the magnets on the rotor was made by the author. This was relatively easy, no magnets were broken, apart from a few during the measurements and in the beginning of the assembly. An anaerobic glue, Loctite326, was used together with an activator.

Magnets with the same polarity placed beside each other in a rotor pole are repelling each other, and the forces can be quite strong, making the gluing of the magnets on the rotor cumbersome. [10] contains safety guidelines for magnet handling. If pieces of magnetic steel are placed above a magnet already glued to the rotor, in such a way that a path is created for the the magnetic flux via the steel piece to the rotor, there will be no or very small repelling forces when a new magnet is glued next to the previous one. The steel pieces are left on until all magnets are glued and the glue is fixed. If the steel pieces are thin there will be more of them needed, but applying and removing them will be easier, as the forces will be lower.

A picture of the rotor with the magnets mounted is shown in figure 5.12.

**Figure 5.12** The rotor, with the magnets mounted but without the retaining layer of kevlar.

## 5.4 Recalculation of drive cycle requirement

When the rotor was assembled, the inertia of the rotor was calculated. The inertia of the different parts can be found in table 5.3.

| Part | Shaft | Washers | Spacer | Nut | Magnets | Tube |
|---|---|---|---|---|---|---|
| Inertia $[kgcm^2]$ | 0.579 | 0.124 | 0.017 | 0.023 | 0.970 | 1.017 |

**Table 5.3** The inertia of the parts of the rotor. The inertia of the washers is the inertia of both washers together.

The inertia of the assembled rotor, $J_{rotor}$, is calculated as the sum of the inertias of the parts.

$$\begin{aligned} J_{rotor} &= J_{shaft} + J_{wash} + J_{dist} + J_{nut} + J_{mag} + J_{tube} \\ &= 2.729 \cdot 10^{-4} \ \ [kgm^2] \end{aligned} \tag{5.1}$$

The inertia on the motor axis, $J_{motor}$, is the sum of the inertia of the rotor, $J_{rotor}$, the resolver, $J_{resolver}$, the brake, $J_{brake}$, and the motor side of the gear, $J_{gear-h}$.

$$\begin{aligned} J_h &= J_{rotor} + J_{resolver} + J_{brake} + J_{gear-h} \\ &= 2.729 \cdot 10^{-4} + 0.120 \cdot 10^{-4} + 1.00 \cdot 10^{-4} + 0.560 \cdot 10^{-4} \\ &= 4.409 \cdot 10^{-4} \ [kgm^2] \end{aligned} \tag{5.2}$$

According to equation 3.20, the maximum acceleration was calculated.

$$\left(\frac{d\omega}{dt}\right)_{max} = \frac{T_{gear} + T_{mg}}{J_{load-eq}} = \frac{6.150 + 2.60}{14.70 \cdot 10^{-4}} = 5952 \ \ [rad/s^2] \tag{5.3}$$

The quantities were according to table 4.1. The accelerating and braking torques were then calculated.

$$\begin{aligned} T_{acc} &= T_{gear} + T_{fric1} + J_h \left(\frac{d\omega}{dt}\right)_{max} \\ &= 6.150 + 2.550 + 5952 \cdot 4.409 \cdot 10^{-4} = 11.324 \ \ [Nm] \end{aligned} \tag{5.4}$$

$$\begin{aligned} T_{dec} &= T_{gear} - T_{fric2} + J_h \left(\frac{d\omega}{dt}\right)_{max} \\ &= 6.150 - 0.400 + 5952 \cdot 4.409 \cdot 10^{-4} = 8.374 \ \ [Nm] \end{aligned} \tag{5.5}$$

The root mean square torque required by the drive cycle was finally calculated according to equation 3.24.

$$\begin{aligned} T_{rms} &= \frac{1}{K_{cool}} \sqrt{\frac{100}{95}} K_{os} \sqrt{(T_{acc})^2 \frac{i}{2} + (T_{dec})^2 \frac{i}{2} + (T_{stat})^2 (1 - i)} \\ &= \frac{1.12}{\sqrt{0.95}} \sqrt{(11.324)^2 \, 0.05 + (8.374)^2 \, 0.05 + (3.390)^2 \, 0.9} = 5.172 \ \ [Nm] \end{aligned} \tag{5.6}$$

The required root mean square torque, not considering armature reaction, was 5.17 Nm.

Due to armature reaction, although the effect is small in this kind of machine, the torque constant $K_t$ will decrease with with higher torque levels, implying that a relatively higher current must be supplied for the machine to produce the desired torque. When $K_t$ drops for higher currents, the torque figures in the formula for $T_{rms}$ must be increased with the relative drop in $K_t$ to reflect the fact that a larger current, with the associated higher resistive losses, must be supplied.

By FEM, $K_t$ was calculated relative its value at 5.17 $Nm$, which is the torque level of the required root mean square torque calculated by equation 5.6.

FEM calculations showed that at $T_{acc} = 11.324 \ Nm$, the drop in $K_t$ is 2.30 %, at $T_{dec} = 8.374 \ Nm$ the drop in $K_t$ is 0.89 %, and at $T_{stat} = 3.390 \ Nm$ $K_t$ is 0.26 % higher than at $T_{rms}$. The torque levels had to be adjusted as follows

$$T_{acc-ar} = 1.023 \cdot 11.324 = 11.584 \ Nm \tag{5.7}$$

$$T_{dec-ar} = 1.0089 \cdot 8.374 = 8.449 \ Nm \tag{5.8}$$

$$T_{stat-ar} = 0.9974 \cdot 3.390 = 3.381 \ Nm \tag{5.9}$$

The root mean square torque, adjusted for armature reaction, $T_{rms-ar}$, was calculated as

$$\begin{aligned} T_{rms-ar} &= \frac{1}{K_{cool}}\sqrt{\frac{100}{95}}K_{os}\sqrt{\left(T_{acc-ar}\right)^2\frac{i}{2}+\left(T_{dec-ar}\right)^2\frac{i}{2}+\left(T_{stat-ar}\right)^2(1-i)} \\ &= \frac{1.12}{\sqrt{0.95}}\sqrt{\left(11.584\right)^2 0.05+\left(8.449\right)^2 0.05+\left(3.381\right)^2 0.9}=5.21 \quad [Nm] \end{aligned} \tag{5.10}$$

The required root mean square torque was 5.21 Nm. This is a 0.75 % increase due to armature reaction.

## 5.5 Data for the optimized geometry

The data for the final design is given in table 5.4.

## 5.6 Comparison old and new design

A comparison of the original machine and the new is shown in figure 5.13. A comparison of selected qualities of the two machines is in table 5.5.

As can be seen in table 5.5, the active length, the nominal torque and speed, the inertia, the magnet volume and the material cost of the new design is reduced substantially compared to the original design.

$$\frac{l_{stack-NEW}}{l_{stack-OLD}} = 0.65 \tag{5.11}$$

$$\frac{T_{nom-NEW}}{T_{nom-OLD}} = 0.91 \tag{5.12}$$

$$\frac{n_{nom-NEW}}{n_{nom-OLD}} = 0.50 \tag{5.13}$$

The active length is reduced to 65 %. The nominal torque is reduced to 91 %, and the nominal speed to 50 %. The new machine is thus a smaller machine than the present, and the comparison can thus be regarded as unfair. However, the optimization of the new machine is done with respect to a specific application, and for that application the comparison is valid.

$$\frac{J_{rot+res-NEW}}{J_{rot+res-OLD}} = 0.44 \tag{5.14}$$

$$\frac{J_{active-NEW}}{J_{active-OLD}} = 0.44 \tag{5.15}$$

| Quantity | Designation | Value |
|---|---|---|
| Number of poles | $2p$ | 10 |
| Number of slots | $Q$ | 30 |
| Slots/pole/phase | $q$ | 1 |
| Active length | $l_{stack}$ | 85 mm |
| Outer diameter | $2r_{sy}$ | 90 mm |
| Inner diameter | $2r_{si}$ | 51.26 mm |
| Airgap | $g$ | 0.5 mm |
| Nominal torque | $T_{nom}$ | 5.17 Nm |
| Nominal speed | $n_{nom}$ | 1650 rpm |
| Nominal current | $I_{nom}$ | 6.81 $A_{rms}$ |
| Torque constant | $K_T$ | 0.76 $Nm/A_{rms}$ |
| Voltage constant | $K_E$ | 42 $V/1000$ $rpm$ |
| Magnet volume | $V_{mag}$ | 20.4 $cm^3$ |
| Magnet price | $\$_{mag}$ | 41.9 p.u. |
| Iron price | $\$_{iron}$ | 7.0 p.u. |
| Copper price | $\$_{copper}$ | 2.5 p.u. |
| Total material price | $\$_{tot}$ | 51.5 p.u. |
| Inertia of rotor | $J_{rotor}$ | 2.73 $kgcm^2$ |
| Magnet height | $h_m$ | 2.50 mm |

**Table 5.4** Properties of the new machine

The inertia is reduced to 44 %, either the whole machines or only the active parts are compared.

$$\frac{V_{mag-NEW}}{V_{mag-OLD}} = 0.71 \tag{5.16}$$

$$\frac{\$_{active-NEW}}{\$_{active-OLD}} = 0.70 \tag{5.17}$$

The magnet material price and volume is reduced to 71 %, and the cost of the material in the active part of the machine is reduced to 70 %.

| Quantity | PS90/6-131 | PS90/10-85 |
|---|---|---|
| Number of poles, $2p$ | 6 | 10 |
| Number of slots, $Q$ | 27 | 30 |
| Slots/pole/phase, $q$ | 1.5 | 1 |
| Active length, $l_{stack}$ | 131 mm | 85 mm |
| Outer diameter, $2r_{sy}$ | 90 mm | 90 mm |
| Inner diameter, $2r_{si}$ | 51.26 mm | 51.26 mm |
| Airgap, $g$ | 0.5 mm | 0.5 mm |
| Nominal torque, $T_{nom}$ | 5.7 Nm | 5.2 Nm |
| Nominal speed, $n_{nom}$ | 3300 rpm | 1650 rpm |
| Inertia of rotor, with resolver, $J_{rot+res}$ | 6.5 $kgcm^2$ | 2.85 $kgcm^2$ |
| Inertia, active part, $J_{active}$ | 5.00 $kgcm^2$ | 2.22 $kgcm^2$ |
| Magnet volume, $V_{mag}$ | 28.9 $cm^3$ | 20.4 $cm^3$ |
| Magnet price, $\$_{mag}$ | 59.3 p.u. | 41.9 p.u. |
| Price, active part, $\$_{active}$ | 72.5 p.u. | 50.5 p.u. |

**Table 5.5** A comparison between the present and the new design.

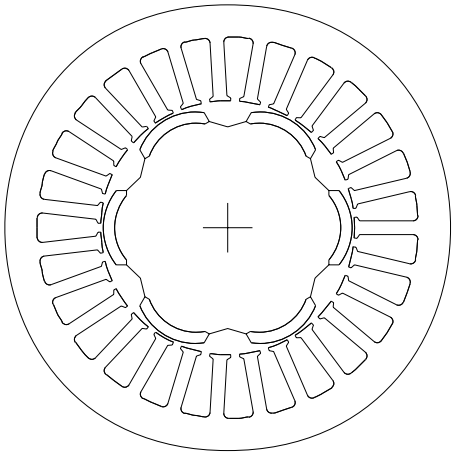

(a) Original crossection.

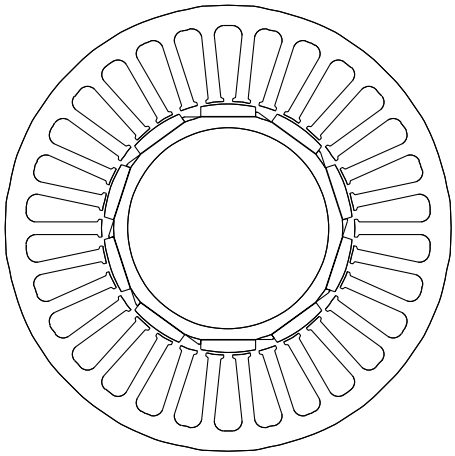

(b) New crossection.

**Figure 5.13** The crossections of the original and the new machine.

# 6

# Measurements

## 6.1 Standard Thermal Test

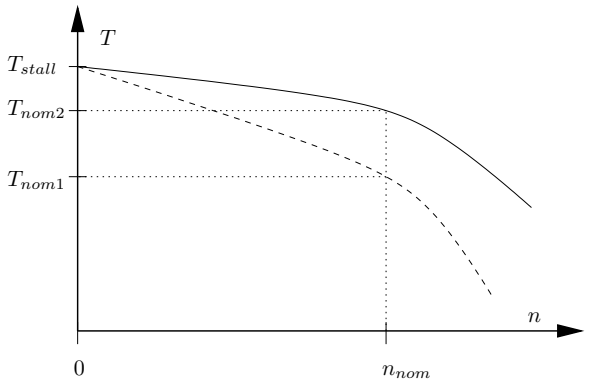


**Figure 6.1** The maximum continuous torque, $T$ versus speed, $n$, for two machines, one with low iron losses (continuous line) and one with higher iron losses (dashed line).

The rated torque for the servo motors in question is determined by a standard thermal test, where the machine is mounted on a steel flange, of dimension $400 \times 400 \times 20$ mm, see appendix E. The machine is run at constant speed and constant torque until thermal steady state is reached, and then the average temperature rise in the windings is measured. The torque that the machine can supply at a maximum temperature rise of $100^\circ\, C$ at rated speed is defined as the nominal torque of the machine. The maximum torque is investigated

for different speeds, and a plot of maximum continuous torque versus speed is usually according to figure 6.1. As these machines lack a cooling fan, they are depending on heat transfer to the structure on which they are mounted and natural convection and radiation for the cooling. The machines can produce more torque at standstill than at nominal speed, due to the absence of iron losses at standstill. In figure 6.1 the torque to speed characteristics of two machines are shown, both having the same stall-torque and nominal speed, but different nominal torque, due to differences in iron losses. The stall-torque is the maximum average torque at standstill.

## 6.2 The laboratory setup

The test setup for the servo motor consisted of a DC-machine coupled to the shaft of the servo motor via a torque transducer, electronics and converters for the control of machines and electronics for measuring the servo motor winding resistance and the torque. See figure 6.2. There were also meters for measuring the temperature in a slot and in an end-turn with thermocouples. An oscilloscope was used to monitor the currents of the servo motor.

The prototype was mounted in a test bench on a steel flange according to section 6.1. The switching frequency of the converter for the prototype was 8.0 kHz, and the bus voltage 275 V.

The torque was measured by a torque-transducer, and the average winding temperature was calculated from the phase resistance.

At first, the winding resistance was measured by an ohm-meter, but this method was not accurate, as the ohm-meter took too long time to measure the resistance. The winding temperature decreased during the measuring period, so not only was the reading inaccurate, it was also difficult to obtain a reading, as the reading dropped continuously during the measurement. The phase resistance was instead obtained by feeding two phases with a DC-voltage, measuring the current through and the voltage over the phases, and then calculating the resistance. The average temperature rise in the winding was calculated with the formula

$$T_{rise} = \frac{R_{measured} - R_{start}}{R_{start}} 255 \tag{6.1}$$

$R_{start}$ is the resistance at the beginning of the test, the room temperature. $R_{measured}$ is the measured resistance during the test, and when $R_{measured}$ is approximately 1.4 times $R_{start}$, the temperature rise is $100^{\circ}\,C$. As the current through the the two excited phases was approximately of the same value

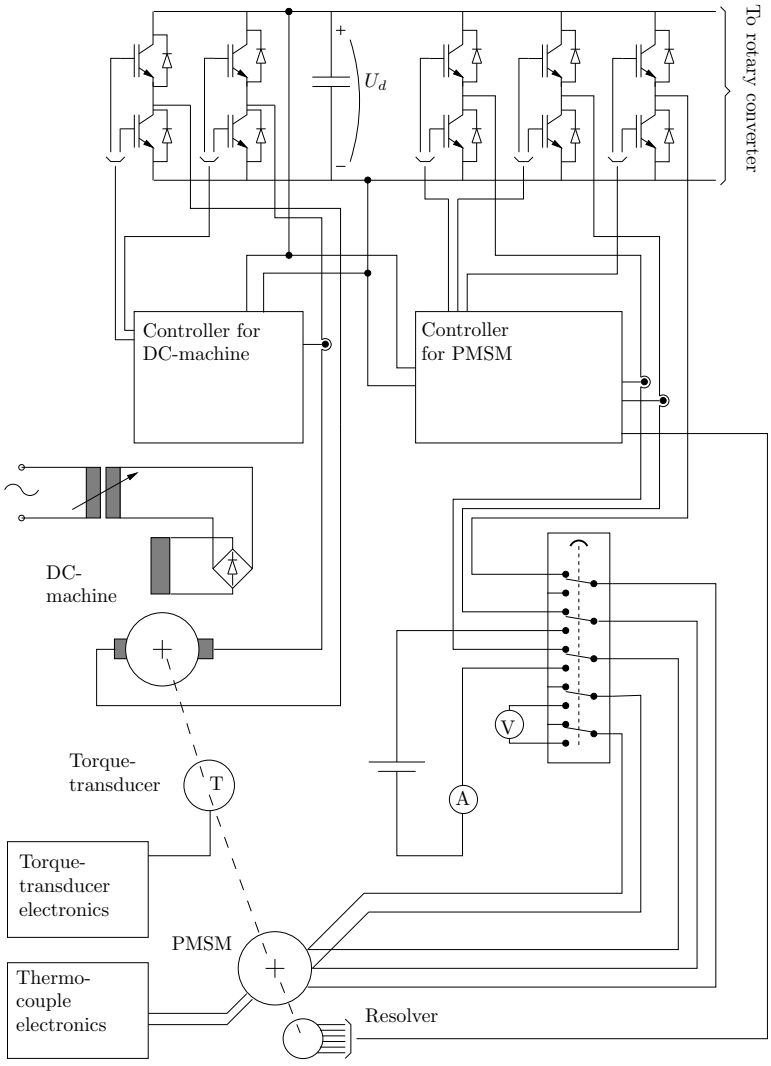


**Figure 6.2** Circuit diagram for the test setup.

as the root mean square value of the phase currents during the running of the machine, the resistive losses were comparable, and therefore the temperature drop during the measurement was not disturbing the measurements. A benefit of the utilized voltage and ampere-meters was that their reading could be locked, which was done simultaneously, so there was no problem of noting their reading. For a continuous approximate reading of the winding temperature, there were two thermocouples inserted in the winding at the manufacturing. One thermocouple was placed in the end connections of the winding, and the other in a slot. The thermocouples were connected to the appropriate electronics during the test.

The speed was measured by a frequency counter connected to the control electronics output for the cosine of the electrical rotor angle.

The phase to neutral and phase to phase voltages were measured by an oscilloscope. The prototype had the star point of the winding available for voltage measurement.

## 6.3 The induced voltage

The induced voltage of the machine was measured, both phase to neutral voltage, and the phase to phase voltage.

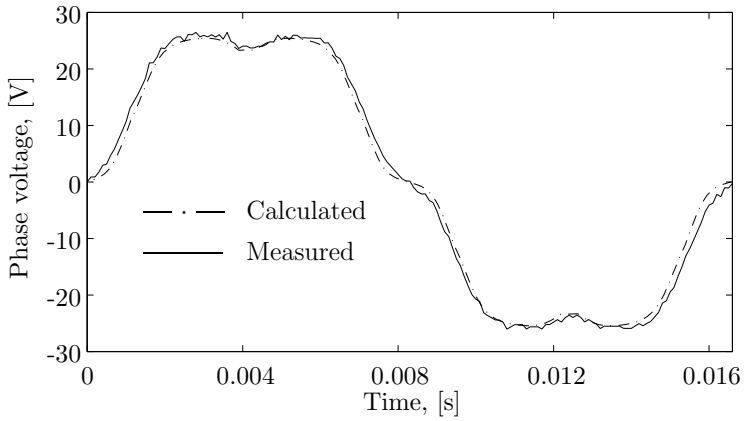


**Figure 6.3** The measured and the calculated induced phase to neutral voltage at 723 rpm.

As can be seen in figures 6.3 and 6.4, the calculated voltages correspond well with the measured. The finite element method gives accurate results.

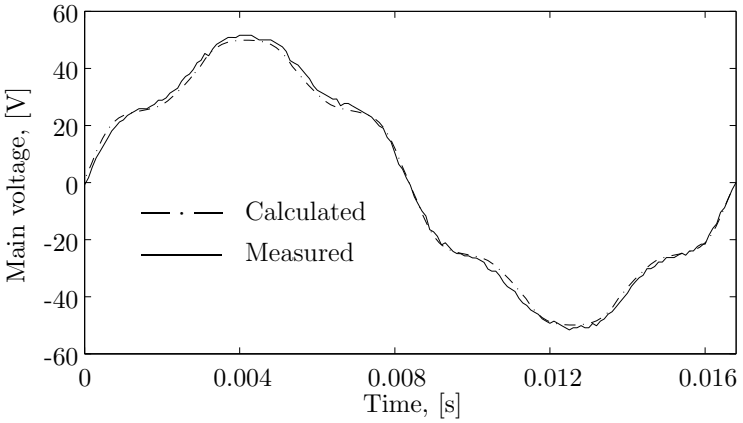


**Figure 6.4** The measured and the calculated induced phase to phase voltage at 714 rpm.

## 6.4 Torque

The torque for a number of different phase currents were measured, and the results are shown in table 6.1 and figure 6.5.

| Current [A] | Motoring torque [Nm] | Generating torque [Nm] | Average torque [Nm] | Kt [Nm/A] | $\Delta K_{t-ar}$ [%] | $\Delta K_{t-opt}$ [%] |
|---|---|---|---|---|---|---|
| 4.0 | 3.07 | 3.14 | 3.11 | 0.7770 | 0.0 | 2.7 |
| 6.0 | 4.61 | 4.71 | 4.66 | 0.7766 | 0.1 | 2.6 |
| 8.0 | 6.13 | 6.25 | 6.19 | 0.7736 | 0.4 | 2.2 |
| 10.0 | 7.63 | 7.76 | 7.69 | 0.7693 | 1.0 | 1.7 |
| 12.0 | 9.09 | 9.24 | 9.16 | 0.7634 | 1.8 | 0.9 |
| 14.0 | 10.61 | 10.71 | 10.66 | 0.7615 | 2.0 | 0.6 |

**Table 6.1** Current, torque and torque constant, $K_t$. The average torque is the average of the motoring and the generating torque for a certain current level.

The measurements were done at 1650 rpm, so there is a difference in the torque for motoring and generating due to friction.

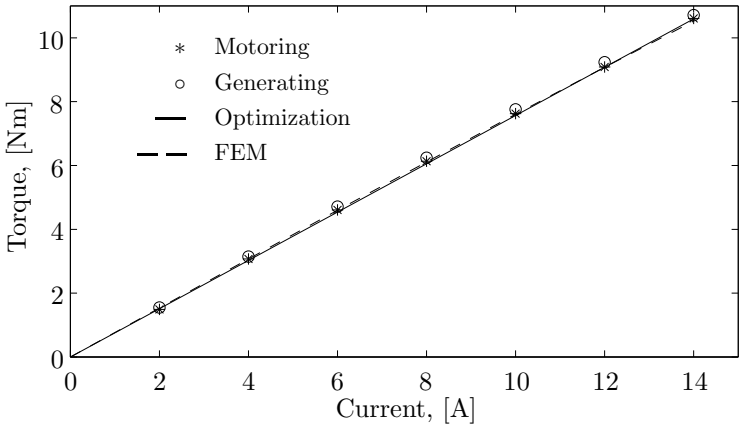


**Figure 6.5** The measured torque at different current levels at 1650 rpm. The measured motoring and the generating torque is compared with the necessary torque according to the optimization and with FEM torque calculation results.

The torque constant in table 6.1, $K_t$, is expressed as

$$K_t(I_{rms}) = \frac{T(I_{rms})}{I_{rms}} \tag{6.2}$$

The relative decrease of $K_t$ in table 6.1, $\Delta K_t$, is calculated as

$$\Delta K_{t-ar}(I_{rms}) = \frac{K_t(4) - K_t(I_{rms})}{K_t(4)} \tag{6.3}$$

The required torque constant from the optimization, $K_{t-opt}$, was 0.757. The difference between $K_{t-opt}$ and the measured $K_t$ is in table 6.1 designated $\Delta K_{t-opt}$, and is calculated as

$$\Delta K_{t-opt}(I_{rms}) = \frac{K_t(I_{rms})}{K_{t-opt}} \tag{6.4}$$

For the torque levels determined by the drive cycle, the measured $K_t$ is higher than the $K_t$ required by the drive cycle.

## 6.5 Inductance measurements

The inductance of the machine was measured between the terminals, and the result is shown in figure 6.6.

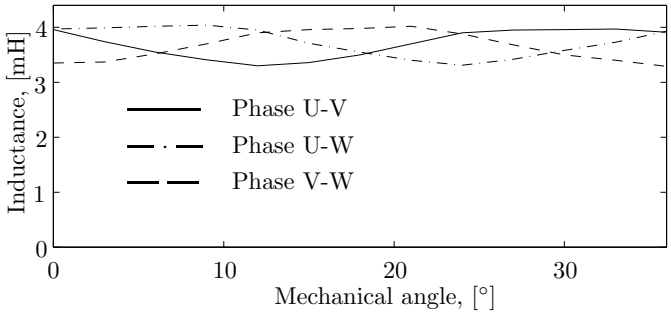


**Figure 6.6** The change of inductance with the rotor position. The inductance is measured terminal to terminal.

The measurements suggest that the rotor is salient. With quadrature current control the saliency is of minor importance, though.

## 6.6 Thermal limit measurements

The results of the torque and temperature measurements are in table 6.2 and figure 6.7.

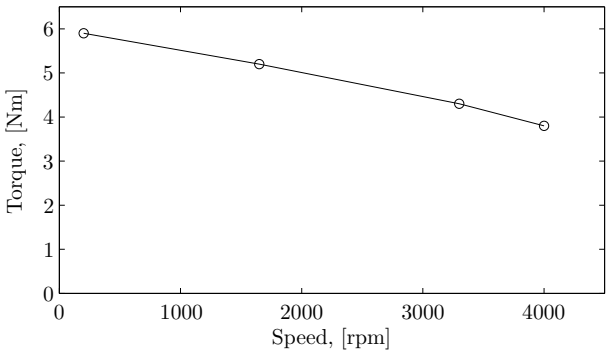


**Figure 6.7** The the maximum torque for different speeds.

The machine was capable of delivering 5.2 Nm at a temperature rise of $100° C$. This is 0.22% less than the root mean square torque demanded by the drive cycle.

| Speed [rpm] | Torque [Nm] | Temperature rise $[^\circ C]$ |
|---|---|---|
| 200 | 5.9 | 104 |
| 1650 | 5.2 | 102 |
| 3300 | 4.3 | 102 |
| 4000 | 3.8 | 106 |

**Table 6.2** The thermal limit at different speeds.

## 6.7 Comments

The finite element analysis results corresponded well with the measured values. It should be noted that as the temperature of the magnets during the measurements is unknown. Therefore there is an uncertainty regarding their remanence during the measurements, which could differ from the value used in the FEM-calculations.

The machine failed to fulfill the *RMS*-torque demand of the drive cycle by 0.22%. The difference is very small, and had the copper fill factor been 0.44% larger, the machine had met the requirements. Note also, that the machine had magnets that were approximately 6% weaker than what is possible to obtain by grinding the magnets properly. With properly ground magnets, the machine would have fulfilled the requirements.

As there is a margin in the calculation of $T_{rms}$ of 12 % due to the oversizing of the present machine, the new design can still meet the demands of the drive cycle if the 12 % margin is adjusted. The comparison with the existing design then becomes less relevant, though.

# 7

# Conclusions and Future Work

## 7.1 Conclusions

A permanent magnet synchronous machine has been optimized for an industrial robot application. The optimization was made with respect to material cost, considering the demands of the application. The optimization yielded a smaller and less expensive machine, compared to the machine presently used in the application. The pole number was increased from 6 to 10. The active length was reduced by 35 %. The nominal torque was reduced by 9 %, and the nominal speed by 50 %. The inertia of the active part of the machine was reduced by 56 %. The magnet material price and volume was reduced by 29 %, and the cost of the material in the active part of the machine was reduced by 30 %. FEM calculations indicate that the machine has a high torque ripple, a peak to peak value of 17 % of the average torque at nominal torque. It is assumed that this torque ripple can be compensated for by current profiling.

A prototype has been built which has the predicted back-EMF, but fails by 0.22% to fulfil the RMS-torque required by the drive cycle. If the copper fill factor had been just slightly higher, the machine would have fulfilled the demands. Due to a manufacturing error the prototype had magnets with approximately 6% lower strength than achievable. With magnets properly manufactured, the goal had been achieved.

The rated speed of the new machine is only half of the rated speed of the present machine. As a consequence it has been favourable to increase the pole number from 6 to 10, without the iron losses becoming too high. A

benefit of increasing the pole number is that the maximum demagnetizing MMF decreases.

It is important to reduce the inertia of the magnetically active parts of the rotor, but it is also important to have a low inertia in mind when designing the other parts of the rotor, as their effect on the inertia can be significant.

The concept of the new machine seems promising. The tube rotor, although more complicated than the present design, reduces material and inertia in an inertia sensitive application. The concept of tapered magnets results in a more simple magnet geometry, and therefore should have lower manufacturing costs.

For the calculation of the flux in the machine, the simple MEC-model presented here seems to work well, although no systematic comparison between the model results and FEM results have been made. The model relies on the assumption of negligible armature reaction, which is true for the PMSM with surface mounted magnets considered here. The torque linearity has to be checked separately by FEM. By the use of the MEC-model, the flux-density in the stator and rotor iron can be varied freely by the optimization routine. Therefore, the optimal tradeoff for the rotor yoke thickness between flux-density and inertia can be made by the optimization routine. In the model, it is also easy to change the pole and the slot number.

For the calculation of the iron losses, a formula was used that both incorporated a part proportional to $\omega_m$ (hysteresis loss) and a part proportional to $\omega_m^2$ (eddy current loss). To be consistent with the concept of a root mean square torque, the loss formula for the iron should be modified to only have dependence on $\omega_m^2$.

The thermal model requires further identification and development. The dependence between permissible losses and the machine size must be investigated further.

The mounting of the magnets on the prototype was easy, using the right methods, even though the magnets were magnetized. It is important to consider the strong forces and brittleness of a magnetized $Sm_2Co_{17}$-magnet, but doing so, there little difficulty in handling them. The origin of the strong attracting (and repelling) forces must be understood, and considering these, effective measures can be taken to neutralise them. It is the belief of the author that automatic gluing of *magnetized* magnets on PMSM-rotors can be made, only the right measures are taken. This should be accompanied by automatic mechanical and magnetic measurement of individual magnet segments, together with a sorting procedure to obtain narrow tolerances in induced voltage and torque ripple.

The measurement of the average winding temperature was more difficult than expected, but finally, the method of measuring voltage and current worked well.

The FEM-results corresponded very well to the measurements. It is important to have in mind that FEM is a complicated tool which requires a competent user and good input data. With a bad mesh and bad material data, the accuracy will deteriorate.

## 7.2 Future work

The iron loss calculation should be modified to be consistent with the concept of a root mean square torque, and the thermal modelling should be improved. Preferably, a FEM or a lumped parameter thermal model should be used, see [5]. The standard test with a steel flange seems like a well defined environment where an effort in the thermal modelling could give good results.

Ideally FEM should be used for the optimization. This would open up the opportunity of including constraints on torque ripple and power requirements of the converter, directly into the optimization. Until now, however, FEM has been regarded as too time consuming for the optimization.

Other optimization objectives could also be investigated, for example, maximizing the torque per unit price for a certain machine volume, or minimizing the volume with constrained minimum torque and maximum cost.

Alternative concepts could also be investigated with the optimization strategy used here. The introduction of soft magnetic composites, see [6], offers the possibility of new machine concepts, which might be suitable for servo motors.

# 8

# References


[1] M.S.Bazaraa H.D.Sherali C.M.Shetty. *Nonlinear programming: Theory and algorithms*. Wiley, 1993.

[2] C.Sadarangani. *Electrical Machine Design: Part 1*. KTH, Stockholm, 1998.

[3] E.Uddeholt. *Identifiering och kompensering av motor- och resolverrippel*. KTH, Stockholm, 1998.

[4] F.Bouillault and C.Marchand. Improvment of servomotors control laws with the help of finite element method. *IEEE Transactions on Magnetics*, 31:2020–2025, May 1995.

[5] G.Kylander. *Thermal modelling of small cage induction motors*. CTH, Göteborg, 1997.

[6] A. G. Jack. Experience with using soft magnetic composites for electrical machines. *IEE Colloquium on New Magnetic Materials - Bonded Iron, Lamination Steels, Sintered Iron and Permanent Magnets*, 3:1–4, May 1998.

[7] J.Holtz and L.Springob. Identification and compensation of torque ripple in high-precision permanent magnet motor drives. *IEEE Transactions on Industrial Electronics*, 42:309–320, April 1996.

[8] J.Luomi. *Magnetic field calculations and electrical machines*. CTH, Göteborg, 1997.

[9] J.Luukko J.Kaukonen M.Niemel O.Pyrhonen J.Pyrhonen. Permanent magnet synchronous motor drive based on direct flux linkage control. In *European Power Electronics Conference, 1997. EPE 97 Record.*, volume 3, pages 3.683–3.688, 1997.

[10] T.J.E.Miller J.R.Hendershot. *Design of Brushless Permanent Magnet Motors*. Clarendon Press, Oxford Science Publications and Magna Physics Publishing, 1994.

[11] L.Harnefors. *On Analysis, Control and Estimation of Variable Speed Drives*. KTH, Stockholm, 1997.

[12] M.Alaküla. *Styrning av elektriska drivsystem*. IEA,LTH, 1991.

[13] G.Slemon P.Pillay. *Performance and Design of Brushless Permanent Magnet AC Motor Drives*. IEEE Industry Applications Society, 1989.

[14] P.Thelin. *Integration Aspects and Development of a Compact 15 kW PM Integral Motor*. KTH, Stockholm, 1999.

[15] R.J.Parker. *Advances in Permanent Magnetism*. Wiley, 1990.

[16] T.Ekman. *Numeriska metoder på dator och dosa*. Studentlitteratur, 1987.

[17] T.M.Jahns and W.L.Soong. Pulsating torque minimization techniques for permanent magnet ac motor drives - a review. *IEEE Transactions on Industrial Electronics*, 43:321–330, April 1996.

[18] V.Ostović. *Dynamics of Staurated Electric Machines*. Springer Verlag, 1989.

[19] A.M.Stanković V.Petrović, R.Ortega and G.Tadmor. An adaptive controller for minimization of torque ripple in pm synchronous motors. In *Power Electronics Specialists Conference, 1998. PESC 98 Record.*, volume 1, pages 113–118, 1998.

# A

# Magnet data

| $B_r$ [T] @ 20°$C$ | | | $H_c$ [kA/m] @ 20°$C$ | | | Temperature |
|---|---|---|---|---|---|---|
| Max. | Typ. | Min. | Max. | Typ. | Min. | coefficient [%/K] |
| 1.07 | 1.04 | 1.01 | 795 | 755 | 675 | -0.035 |

**Table A.1** Magnetic properties for the material **S3/225**.

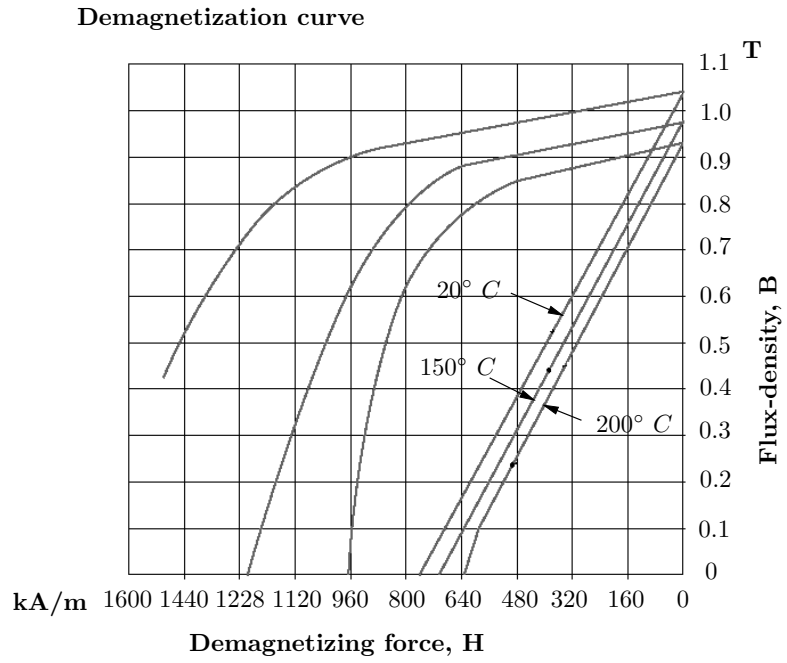


**Figure A.1** The BH-curve for the material **S3/225**.

# B

# Calculation of iron losses

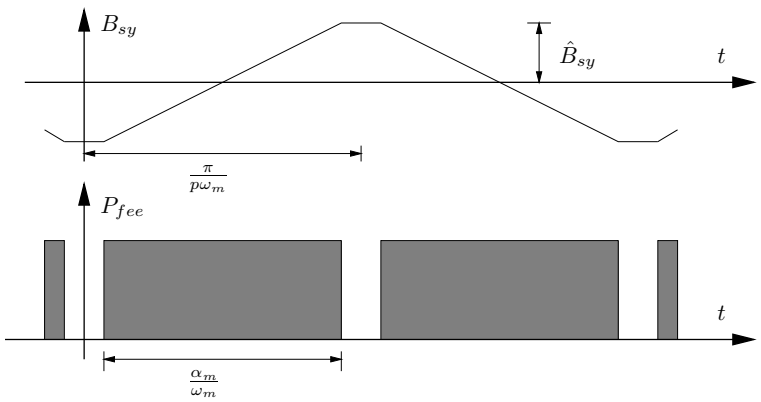


**Figure B.1** The varying flux in the stator yoke, $B_{sy}$, and the associated eddy-current loss, $P_{fee}$.

The eddy current and hysteresis losses in the rotor is neglected. Neither is the iron losses caused by the current ripple at the converter switching frequency accounted for. With a sinusoidally varying flux-density, the iron loss power, $P_{fe}$, per iron mass, $M_{fe}$, can be written

$$\frac{P_{fe}}{M_{fe}} = C_e \hat{B}^2 \omega^2 + C_h \hat{B}^{n(\hat{B})} \omega \tag{B.1}$$

See [10]. The equation consists of one part for the eddy current losses and one part for the hysteresis losses. The constants $C_e$ and $C_h$ are material dependent and must be determined experimentally. The exponent $n(\hat{B})$ is both depending on $\hat{B}$ and the material. The manufacturer of the electrical

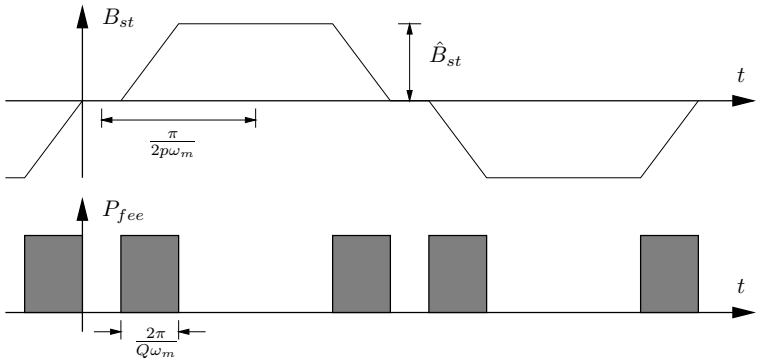


**Figure B.2** The varying flux in a stator tooth, $B_{st}$, and the associated eddy-current loss, $P_{fee}$.

steel can often provide data for the loss per weight for sinusoidal excitation, from which the constants can be calculated.

The hysteresis losses *per cycle* are only depending on the peak value of the varying flux. The eddy current losses *per cycle* are however proportional to the frequency or the rate of change of the flux density, so the eddy current part of equation B.1 can be rewritten, see [13], as

$$C_e \hat{B}^2 \omega^2 = 2C_e \left( \frac{dB(t)}{dt} \right)^2 \frac{t_{loss}}{T} \tag{B.2}$$

This is important, as the flux density variation in the stator is varying according to figure 3.6, and not sinusoidally as assumed for equation B.1, see figure B.1 and B.2. $\frac{t_{loss}}{T}$ is the duty cycle of the eddy current losses, i.e. the relative part of the cycle time that the eddy current losses are produced. For the stator yoke, the derivative of the flux density can be written

$$\frac{dB(t)}{dt} = \frac{2\hat{B}_{sy}}{\frac{\alpha_m}{\omega_m}} = \frac{2\omega_m}{\alpha_m} \hat{B}_{sy} \tag{B.3}$$

The duty cycle of the losses is

$$\frac{t_{loss}}{T} = \frac{\frac{\alpha_m}{\omega_m}}{\frac{\pi}{p\omega_m}} = \frac{p\alpha_m}{\pi} \tag{B.4}$$

Utilising the root mean square speed for the drive cycle, $\omega_{rms}$, the loss per

mass for the stator yoke will be

$$\frac{P_{feye}}{M_{sy}} = 2C_e \left( \frac{2\omega_{rms}}{\alpha_m} \hat{B}_{sy} \right)^2 \frac{p\alpha_m}{\pi} = \frac{8}{\pi\alpha_m} C_e p \omega_{rms}^2 \hat{B}_{sy}^2 \quad \text{(B.5)}$$

For the stator teeth, the derivative of the flux density can be written

$$\frac{dB(t)}{dt} = \frac{\hat{B}_{st}}{\frac{2\pi}{Q\omega_m}} = \frac{Q\omega_m}{2\pi} \hat{B}_{st} \quad \text{(B.6)}$$

The duty cycle of the losses is

$$\frac{t_{loss}}{T} = \frac{\frac{2\pi}{Q\omega_m}}{\frac{\pi}{2p\omega_m}} = \frac{4p}{Q} \quad \text{(B.7)}$$

Utilising the root mean square speed for the drive cycle, $\omega_{rms}$, the loss per mass for the stator teeth will be

$$\frac{P_{fete}}{M_{st}} = 2C_e \left( \frac{Q\omega_{rms}}{2\pi} \hat{B}_{st} \right)^2 \frac{4p}{Q} = \frac{2Q}{\pi^2} C_e \, p \, \omega_{rms}^2 \hat{B}_{st}^2 \quad \text{(B.8)}$$

The hysteresis loss per mass for the stator yoke and the stator teeth will be

$$\frac{P_{feyh}}{M_{sy}} = C_h \hat{B}_{sy}^{n(\hat{B}_{sy})} \overline{\omega}_m \quad \text{(B.9)}$$

$$\frac{P_{feth}}{M_{st}} = C_h \hat{B}_{st}^{n(\hat{B}_{st})} \overline{\omega}_m \quad \text{(B.10)}$$

$\overline{\omega}_m$ is the average speed of the drive cycle. The loss figures from the manufacturer is given in *power per mass* in the unit $[W/kg]$. Therefore, to obtain the loss in *power per volume* the power per mass coefficients must be multiplied with the density of the laminated iron, $\rho_{fe}$, and the iron fill or stacking factor, $k_{ffe}$. $V_{sy}$ is the volume of the stator yoke and $V_{st}$ is the volume of the stator teeth. The total iron losses in the machine is finally

$$\begin{aligned} P_{fe} &= \rho_{fe} k_{ffe} \left( \frac{P_{feye}}{M_{sy}} V_{sy} + \frac{P_{fete}}{M_{st}} V_{st} + \frac{P_{feyh}}{M_{sy}} V_{sy} + \frac{P_{feth}}{M_{st}} V_{st} \right) \\ &= \rho_{fe} k_{ffe} V_{sy} \left( \frac{8}{\pi\alpha_m} C_e p \omega_{rms}^2 \hat{B}_{sy}^2 + C_h \hat{B}_{sy}^{n(\hat{B}_{sy})} \overline{\omega}_m \right) \\ &+ \rho_{fe} k_{ffe} V_{st} \left( \frac{2Q}{\pi^2} C_e \, p \, \omega_{rms}^2 \hat{B}_{st}^2 + C_h \hat{B}_{st}^{n(\hat{B}_{st})} \overline{\omega}_m \right) \end{aligned} \quad \text{(B.11)}$$

# C

# Demagnetization margin

## C.1 Magnet property

The magnets in the machine has to be properly protected against demagnetization. Demagnetization of a magnet will occur if the demagnetizing MMF pushes the magnet below the 'knee' in its BH-curve, see figure C.1. The magnet grade **S3/225** has the 'knee' in its BH-curve in the third quadrant at $20°C$, but as temperature increases, the 'knee' moves up into the second quadrant, see figure A.1.

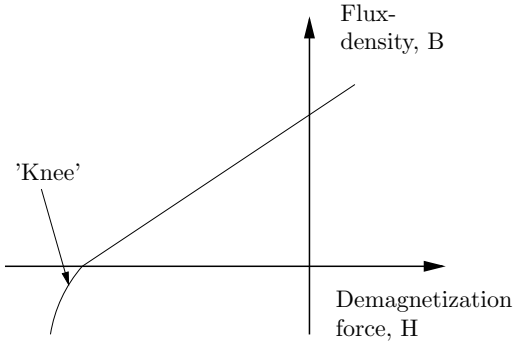


**Figure C.1** The 'knee' in the BH-curve for a magnet material.

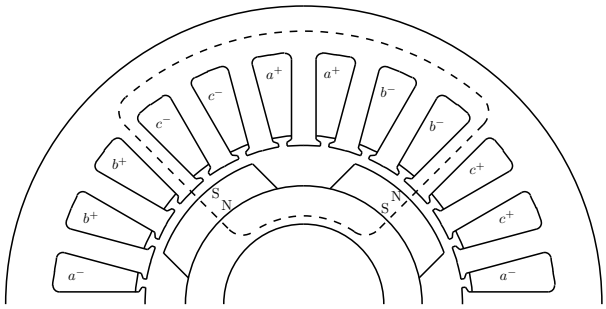


**Figure C.2** The path to calculate the demagnetizing MMF.

## C.2 Maximum demagnetizing current

The maximum demagnetizing current is calculated along the path in figure C.2. To find the current angle which gives the largest total demagnetization current, the current vector is varied in the interval $\left\{-\frac{\pi}{3};+\frac{\pi}{3}\right\}$, according to figure C.3.

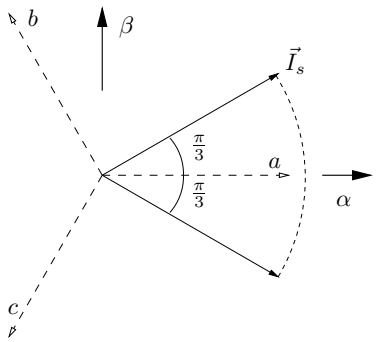


**Figure C.3** The variation of the current vector in the calculation of the maximum demagnetizing MMF. The reference directions for the $\alpha\beta$-axes and the phases $a, b$ and $c$ are displayed.

With the winding star-connected, $i_a + i_b + i_c = 0$, the currents can be written as

$$i_a = N\hat{I}\cos(\theta) \quad i_b = N\hat{I}\cos\left(\theta - \frac{2\pi}{3}\right) \quad i_c = N\hat{I}\cos\left(\theta - \frac{4\pi}{3}\right) \quad \text{(C.1)}$$

The maximum demagnetizing MMF, $F_{max}$, in the rotor position according to figure C.2, including the sign of the current due to the winding distribution according to figure C.2, will be

$$\begin{aligned} F_{max}(\theta) &= N\hat{I}\cos(\theta) - N\hat{I}\cos\left(\theta - \frac{2\pi}{3}\right) - N\hat{I}\cos\left(\theta - \frac{4\pi}{3}\right) \\ &= 2N\hat{I}\cos(\theta) \end{aligned} \tag{C.2}$$

The maximum demagnetizing MMF, $F_{max2}$, demagnetizing *two* magnets, is

$$F_{max2} = 2N\hat{I} \tag{C.3}$$

The MMF per magnet will then be

$$F_{max} = N\hat{I} \tag{C.4}$$

## C.3 Minimum magnet height

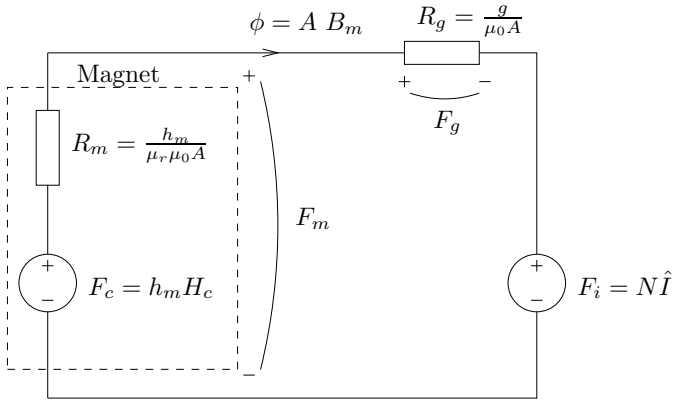


**Figure C.4** Equivalent magnetic circuit of the magnet, airgap and the demagnetizing MMF.

An magnetic equivalent circuit (MEC) of a magnet, the associated airgap and demagnetizing MMF is in figure C.4. The MEC models a flux-tube, see [18], that encloses the path in figure C.2. The flux-tube has an infinitely small cross-sectional area, $A$, and as the flux, $\phi$, is constant in the flux-tube, the flux-density, $B_m$, becomes constant as well. The magnet is here modelled

as an MMF, $F_c$, in series with a reluctance, $R_m$. Note that the reference direction of the MMF over the whole magnet, $F_m$, has opposite direction compared to figure A.1 and C.1. The flux and the flux-density has the same reference direction though. The equation for the MMF around the circuit is

$$F_c - R_m\phi - R_g\phi - F_i = 0 \tag{C.5}$$

The reluctances and the MMF's can be written

$$\begin{aligned} F_c &= h_m H_c && \text{(C.6)} \\ F_i &= N\hat{I} && \text{(C.7)} \\ R_m &= \frac{h_m}{\mu_r\mu_0 A} && \text{(C.8)} \\ R_g &= \frac{g}{\mu_0 A} && \text{(C.9)} \\ \phi &= A\,B_m && \text{(C.10)} \end{aligned}$$

When equation C.5 is rewritten using equations C.6 to C.10, an expression for the magnet height corresponding to a certain flux-density, airgap and demagnetizing MMF is obtained.

$$\begin{aligned} h_m H_c - AB_m\frac{h_m}{\mu_r\mu_0 A} &= AB_m\frac{g}{\mu_0 A} + N\hat{I} && \text{(C.11)} \\ &\Downarrow \\ h_m &= \frac{N\hat{I} + B_m\frac{g}{\mu_0}}{H_c - \frac{B_m}{\mu_r\mu_0}} && \text{(C.12)} \end{aligned}$$

This equation calculates at what MMF the demagnetization process starts. In reality, a margin to demagnetization is required, and therefore the MMF is multiplied with a demagnetization safety factor, $K_{demag}$. The minimum tolerable magnet height can now be calculated as

$$h_{m-min} = \frac{K_{demag}N\hat{I} + B_{m-min}\frac{g}{\mu_0}}{H_c - \frac{B_{m-min}}{\mu_r\mu_0}} \tag{C.13}$$

$N\hat{I}$ is the maximum peak phase current at normal operation, and the demagnetization margin is related to that current. $B_{m-min}$ is the minimum tolerable flux-density in the magnets due to risk of demagnetization.

# D

# Thermal constraints

As the thermal properties of the machine puts a limit on the maximum permissible losses, the maximum allowable iron and copper losses needs to be determined. In [5] a detailed lumped-parameter thermal model is presented for a totally enclosed fan cooled induction motor. This model was regarded as too complicated and time consuming to use, a number of the parameters must be determined experimentally. Instead a formula presented in [2] was used, see equation D.1. The formula calculates the temperature rise in a machine as a function of the losses. No dimensions are included, so the constant $C_{therm}$ varies from machine to machine.

$$\Delta T = C_{therm}\sqrt{P_{cu1}\left(P_{cu1}+P_{cu2}+P_{fe}\right)} \tag{D.1}$$

$P_{cu1}$ and $P_{cu2}$ are the copper losses in the stator and rotor respectively, and $P_{fe}$ is the iron losses. The losses in the rotor of the permanent magnet machine is neglected, so equation D.1 simplifies to D.2.

$$\Delta T = C_{therm}\sqrt{P_{cu}\left(P_{cu}+P_{fe}\right)} \tag{D.2}$$

$P_{cu1}$ and $P_{fe}$ are the copper and iron losses in the stator. As the outer diameter of the motor was fixed during the optimization, equation D.2 had to be adapted for a variable length of the machine. Data for three machines of different lengths of the present design was used. Data for the current causing an approximately $100^{\circ}\,C$ temperature rise for the three machines running at 150 $rpm$ was available. At 150 $rpm$ the iron losses are assumed neglectible, so the temperature rise is only determined by the copper losses, and the thermal constant can be calculated as

$$C_{therm} = \frac{\Delta T}{P_{cu}} \tag{D.3}$$

There seemed to be an relationship between $C_{therm}$ and $\sqrt{l_{stack}}$, so if equation D.3 was modified according to equation D.4, approximately the same $C_{therm}$ was obtained for the three lengths.

$$C_{therm} = \frac{\Delta T}{P_{cu}}\sqrt{l_{stack}} \tag{D.4}$$

The constraint for the maximum losses was then set to

$$\sqrt{P_{cu}\left(P_{cu}+P_{fe}\right)} < \Delta T_{max}\frac{\sqrt{l_{stack}}}{C_{therm}} \tag{D.5}$$

$\Delta T_{max}$ is the maximum allowed temperature rise, here $100°C$.

# E

# Test flange

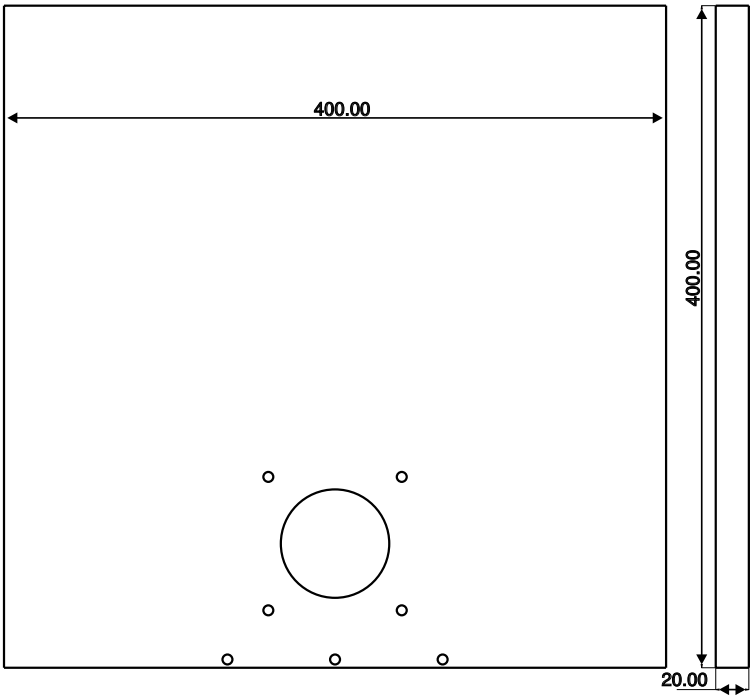


**Figure E.1** The flange for the thermal test, $400 \times 400 \times 20$ mm. The holes are for the mounting of the motor. The material is *RAEX 355*.